Supporting Information for

On the Mechanism of the Stereoselective α-Alkylation of Aldehydes Driven by the Photochemical Activity of Enamines

Ana Bahamonde[†] and Paolo Melchiorre*[,†,‡]

[†]ICIQ - Institute of Chemical Research of Catalonia - the Barcelona Institute of Science and Technology, Av. Països Catalans 16, 43007 Tarragona, Spain.

[‡]ICREA - Catalan Institution for Research and Advanced Studies, Pg. Lluís Companys 23, 08010 Barcelona, Spain.

*Correspondence to: pmelchiorre@iciq.es

Table of Contents

A. General Information **S3**

B. General Procedures for the Photochemical Organocatalytic Enantioselective Alkylation **S4**

C. Optical Absorption Spectra **S5**
C1. Ground State Spectroscopic Studies of the Reaction Mixture in MTBE S5
C2. EDA Complex Formation with the Preformed Enamine **4** S8

D. Characterization of EDA Complexes **S9**
D1. Stoichiometry of the EDA Complex in Solution S9
D2. Determination of the Association Constant (K_{EDA}) S9

E. Mechanistic Studies on the Direct Photoexcitation of Enamines **S11**
E1. Absorption and Emission Spectrum of the Preformed Enamine **4** S11
E2. Stern-Volmer Quenching Studies with Bromomalonate **2c** S13
E3. Electrochemical Analysis of the Preformed Enamine **4** S16

F. Studies on the Catalyst Degradation **S19**
F1. Evolution of the Catalyst Concentration over Time under the Optimal Conditions S19
F2. Evolution of the Catalyst Concentration Irradiating with Monochromatic Light S20
F3. Evolution of the Catalyst Concentration sung *in situ* Irradiation S21

G. Quantum Yield Measurements **S23**
G1. Quantum Yield Measurement for the EDA Complex-Mediated Reactions with **2a** and **2b** S23
G2. Quantum Yield of the Initiation Step for the EDA Complex-Mediated Reactions S25
G3. Quantum Yield Measurement for the Alkylation with Bromomalonate **2c** S26
G4. Quantum Yield of the Initiation Step for the Alkylation with Bromomalonate S27

H. Investigating the Equilibrium of Enamine Formation **S27**
H1. Determination of the Equilibrium Constant ($K_{enamine}$) S27
H2. Effect of the EDA Complex Formation on the Enamine Equilibrium S29

I. Kinetic Studies **S32**
I1. Kinetic Studies for the EDA Complex-Mediated Alkylation of Butanal with **2a** S32
I2. Kinetic Studies for the EDA Complex-Mediated Alkylation of Butanal with **2b** S37
I3. Kinetic Studies for the Alkylation of Butanal with **2c** S40

J. Cyclic Voltammetry **S43**

K. Characterization of the Iminium Ion IX **S45**

L. References **S46**

A. General Information

The NMR spectra were recorded at 400 MHz or 500 MHz for ^{1}H and at 100 MHz or 125 MHz for ^{13}C, respectively. The chemical shifts (δ) for ^{1}H and ^{13}C are given in ppm and are internally referenced to residual protio solvent signals (for $CDCl_3$ @ 7.26 ppm and 77.0 ppm, respectively; for CD_3CN @ 1.96 ppm ^{1}H NMR, 118.26 ppm and 1.79 ppm ^{13}C NMR). Coupling constants are given in Hz. When necessary, ^{1}H and ^{13}C signals were assigned by means of g-COSY 2D-NMR sequence. The following abbreviations are used to indicate the multiplicity: s, singlet; d, doublet; t, triplet; q, quartet; qn, quintet; m, multiplet; bs, broad signal. Optical rotations are reported as follws: $[\alpha]^{rt}_{D}$ (c in g per 100 mL, solvent). Mass spectra (high and low resolution) were obtained from the ICIQ High Resolution Mass Spectrometry Unit on a Bruker Maxis Impact (QTOF) or Waters Micromass LCT-Premier (TOF) in Electrospray Ionization (ESI) by direct infusion. UV-vis measurements were carried out on a Shimadzu UV-2401PC spectrophotometer equipped with photomultiplier detector, double beam optics and D_2 and W light sources. Cyclic voltammetry studies was carried out on a Princeton Applied Research PARSTAT 2273 potentiostat offering compliance voltage up to ± 100 V (available at the counter electrode), ± 10 V scan range and ± 2 A current range.
Cut off and band-pass photochemical experiments have been performed using a 300 W xenon lamp (commercialized under the name of Max-303, *Asashi* Spectra Co., Ltd.) to irradiate the reaction mixture. *In situ* irradiation inside the NMR spectrometer was performed using a 150 W xenon lamp coupled to a monochromator. Commercialized under the name of Polychrome V, it was purchased from Till Photonics. It is a monochromatizing device with an integrated light source. The wavelength (320-680 nm) delivered by the Polychrome V is controlled from a computer and the monochromatic light is conducted directly into the NMR tube by an Optic Fiber probe. The bandwidth and intensity of the light can be adjusted.

General Procedures. All reactions were set up under an argon atmosphere in oven-dried glassware using standard Schlenk techniques, unless otherwise stated. Synthesis grade solvents were used as purchased and the reaction mixtures were deoxygenated by three cycles of freeze-pump-thaw. Chromatographic purification of products was accomplished using flash chromatography (FC) on silica gel (35-70 mesh). For thin layer chromatography (TLC) analysis throughout this work, Merck precoated TLC plates (silica gel 60 GF_{254}, 0.25 mm) were employed, using UV light as the visualizing agent and an acidic mixture of para-anisaldehyde or basic aqueous potassium permangante ($KMnO_4$) stain solutions, and heat as developing agents. Organic solutions were concentrated under reduced pressure on a Büchi rotatory evaporator.

Determination of Enantiomeric Purity: HPLC analysis on chiral stationary phase was performed on an Agilent 1200-series instrument. Daicel Chiralpak IA or IC columns with hexane:iPrOH or hexane:iPrOH:DCM as the eluents were used. HPLC traces were compared to racemic samples of products **3a-c** prepared using a catalytic amount of morpholine (30 mol%).

Materials. Reagents were purchased at the highest commercial quality from Sigma Aldrich, Fluka, and Alfa Aesar and used as received, without further purification, unless otherwise stated.
The chiral secondary amine catalyst *(S)*-**A** is commercially available; catalyst *(S)*-**A** was purified by column chromatography (from pure hexane to hexane:Et_2O 1:1) prior to use and stored at 4 °C under argon to avoid desilylation of the tertiary alcohol. Both phenacyl bromide (**2b**) and diethyl bromomalonate (**2c**) are commercially available as well as butanal (**1a**). They were vacuum distilled prior to use. 2,4-Dinitrobenzyl bromide (**2a**) was prepared upon bromination of the commercially available 2,4-dinitrotoluene **5**, according to literature (*1*). Enamine **4** was synthesized by condensation of the chiral amine **A** and the commercially available 2-phenylacetaldehyde according to literature (*2*).

B. General Procedures for the Photochemical Organocatalytic Enantioselective Alkylation

A 10 mL Schlenk tube was charged with the aminocatalyst *(S)*-**A** (20 mol%), MTBE (0.5 M referring to the alkyl bromide **2**), butanal **1a** (3 equiv), 2,6-lutidine (1 equiv) and the alkylating agents **2a-c** (1 equiv). The reaction mixture was degassed via freeze pump thaw (x3), and the vessel back-filled with argon. The vial was then sealed and positioned approximately 5 cm away from a light source. After stirring for the indicated time, the crude mixture was purified by flash column chromatography to afford the title compounds **3a-c** in the stated yield and optical purity.

Purification by flash column chromatography on silica gel:
Compound **3a**: gradient eluent from pure hexane to 9:1 hexane:AcOEt.
Compound **3b**: gradient eluent from pure hexane to 95:5 hexane:AcOEt.
Compound **3c**: 10:1 hexane:AcOEt.

The enantiomeric excess was determined by HPLC analysis using the following conditions:
Compound **3a**: Daicel Chiralpak IC column, 70:30 hexane:^{i}PrOH, flow rate 1.00 mL/min, λ = 254 nm: τ_{minor} = 16.7 min, τ_{major} = 19.9 min.

Compound **3b**: Daicel Chiralpak IA column, 98:2 hexane:^{i}PrOH, flow rate 1.00 mL/min, λ = 254 nm: τ_{minor} = 12.0 min, τ_{major} = 13.4 min.

Compound **3c**: Daicel Chiralpak IA column, eluent 97:3 hexane:^{i}PrOH, flow rate 1.00 mL/min, λ = 215 nm:, τ_{minor} = 8.6 min, τ_{major} = 9.3 min.

Products **3a**, **3b**, and **3c** were fully characterized and the data corresponds with literature (*2*, *3*).

Light Sources used in these studies:
- CFL light: A set of two household full spectrum 23 W compact fluorescent light (CFL) bulbs were used for irradiating the reaction mixture (see Figure S1 for the emission).
- Blue LED (λ_{max} = 450 nm): Commercialized under the name of blue LED Emitter LZ4-00B208. It was purchase from LED Engin. The LZ4-00B208 Blue LED emitter is a set of 4 single LEDs which provides 10W power centered at 450 nm. The irradiance at 2 cm of distance was 90.6 mW/cm^2.

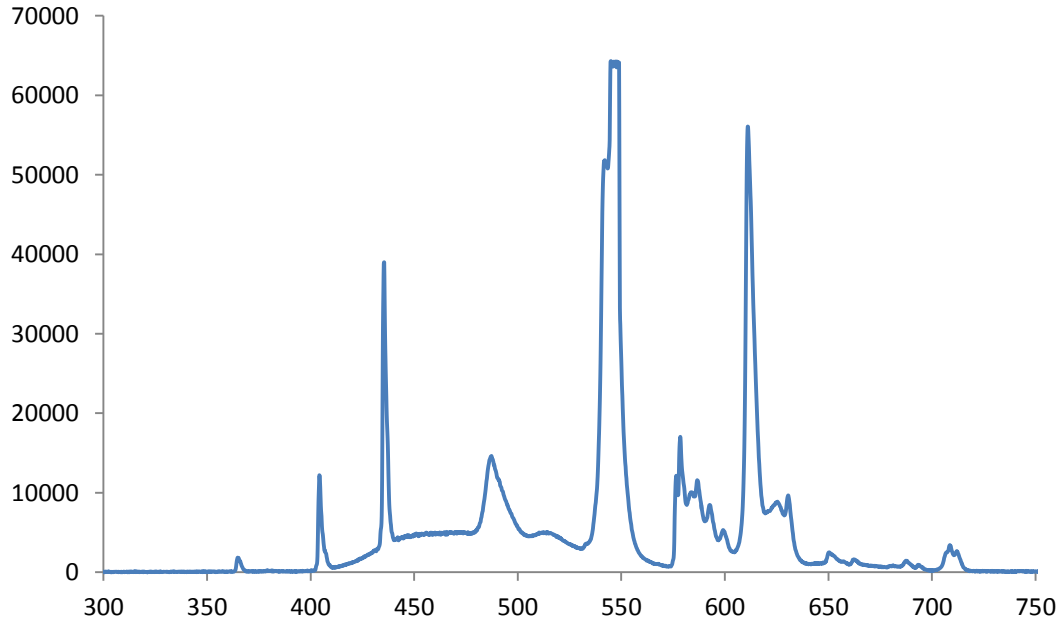

Figure S1: Emission spectra of the 23 W CFL lamp used in our experiments

C. Optical Absorption Spectra

All the spectra were recorded in MTBE, using the same concentration as in the reaction conditions, in a 1 mm Hellma Quartz SUPRASIL® cuvette. Due to the high concentration of the solutions, short path cuvettes were employed in order to avoid signal saturation.

C1. Reaction Mixture in MTBE

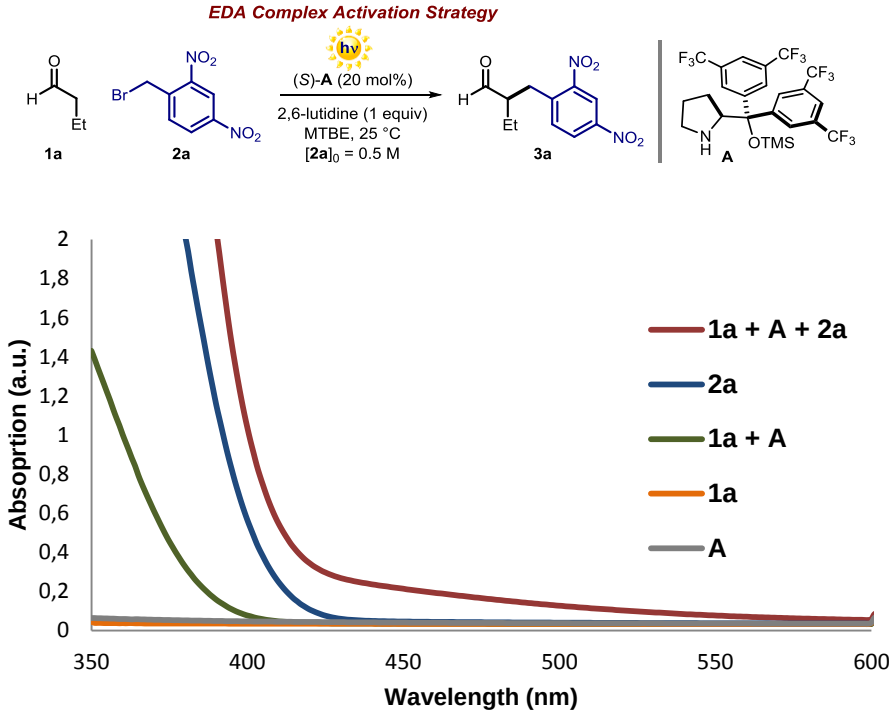

Figure S2. Optical absorption spectra, recorded in MTBE, of the alkylation of butanal **1a** with 2,4-dinitrobenzylbromide **2a**. [**1a**] = 1.5 M: 27.0 µL dissolved in 200 µL of MTBE; [**2a**] = 0.5 M: 26 mg dissolved in 200 µL of MTBE; [*(R)*-**A**] = 0.1 M: 11.9 mg dissolved in 200 µL of MTBE. **1a** + **A**: solution of 27.0 µL of **1a** and 11.9 mg of **A** in 200 µL of MTBE. Mixture of all the reagents: solution of 27.0 µL of **1a**, 11.9 mg of **A** and 26 mg of **2a** in 200 µL of MTBE.

Upon mixing the aldehyde **1a** and the aminocatalyst **A**, a new absorption band is observed (green line in Figure S2), indicating the formation of a transient species: the enamine. The absorption spectrum is analogous to the ones recorded for similar tertiary enamines derived from aliphatic aldehydes, as reported in the literature (*4*). The absorption spectrum of the mixture of all the reagents (red line in Figure S2) does not overlap with the absorption of the enamine (green line). Indeed, a new absorption band is observed. The new absorption band corroborates the formation of an electron donor acceptor (EDA) complex (*5*).

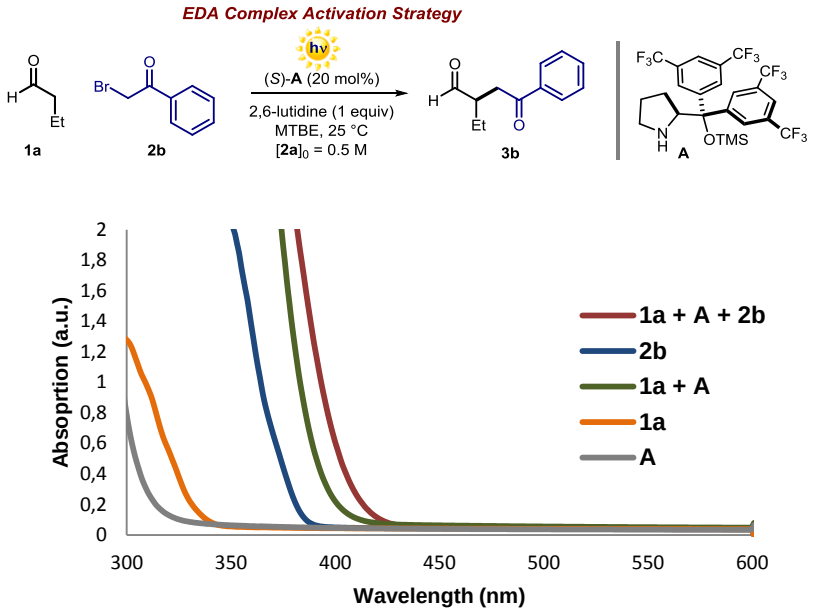

Figure S3. Optical absorption spectra, recorded in MTBE, of the alkylation of butanal **1a** with phenacyl bromide **2b**. [**1a**] = 1.5 M: 27.0 µL dissolved in 200 µL of MTBE; [**2b**] = 0.5 M: 20 mg dissolved in 200 µL of MTBE; [**A**] = 0.2 M: 23.8 mg dissolved in 200 µL of MTBE. **1a** + **A**: solution of 27.0 µL of **1a** and 23.8 mg of **A** in 200 µL of MTBE. Mixture of all the reagents: solution of 27.0 µL of **1a**, 23.8 mg of **A** and 20 mg of **2b** in 200 µL of MTBE.

When recording the optical absorption spectrum in the presence of **2b**, the mixture of all the reagents (red line Figure in S3) does not overlie the absorption of the enamine (green line in Figure S3), and a new absorption band is observed. This new absorption band is diagnostic of an EDA complex formed in the ground state.

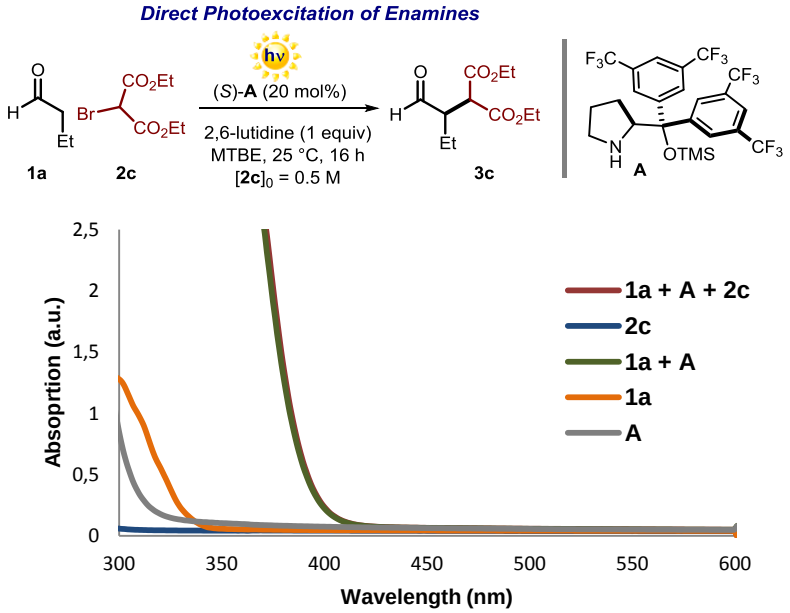

Figure S4. Optical absorption spectra, recorded in MTBE, of the alkylation of butanal **1a** with bromomalonate **2c** driven by the direct excitation of enamines. [**1a**] = 1.5 M: 27.0 µL dissolved in 200 µL of MTBE; [**2c**] = 0.5 M: 17 µL dissolved in 200 µL of MTBE; [**A**] = 0.1 M: 11.9 mg dissolved in 200 µL of MTBE. **1a** + **A**: solution of 27.0 µL of **1a** and 23.8 mg of **A** in 200 µL of MTBE. Mixture of all the reagents: solution of 27.0 µL of **1a**, 11.9 mg of **A** and 17 µL of **2c** in 200 µL of MTBE.

Upon mixing the aldehyde **1a** and the aminocatalyst **A**, a new absorption band is observed (*in situ* generated enamine, green line in Figure S4). The optical absorption spectrum of the reaction mixture (red line in Figure S4) perfectly overlays the absorption of the enamine (green line), excluding any EDA association in the ground state.

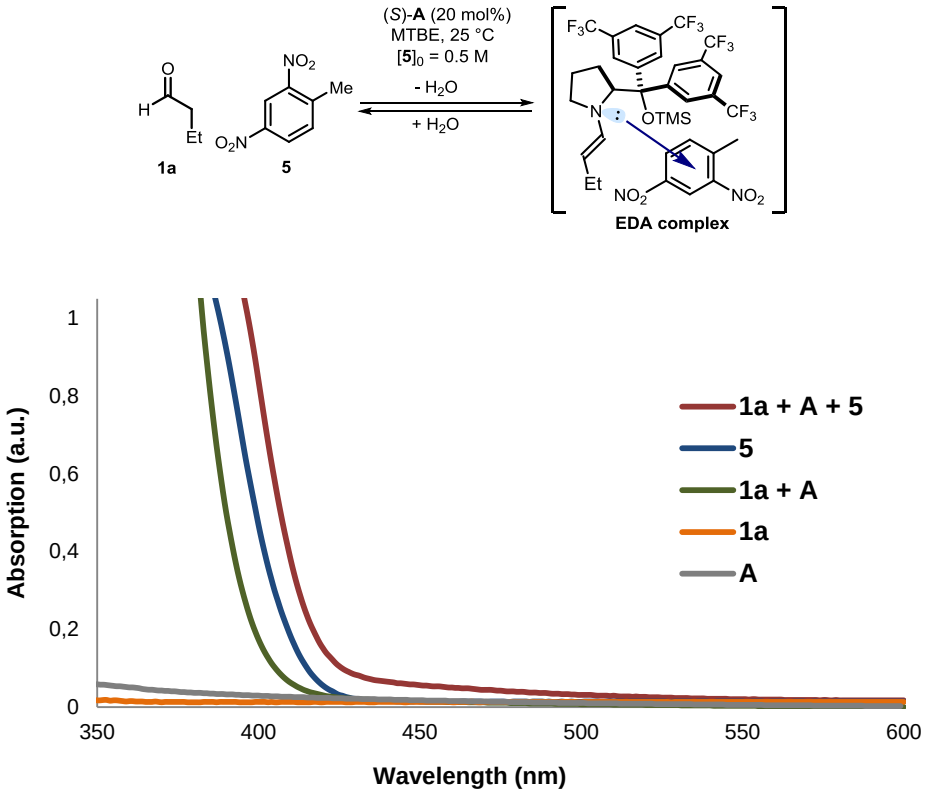

Figure S5. Absorption spectra of the 2,4-dinitrotoluene **5** (blue line) and comparison of the mixture aldehyde **1a** + catalyst **A** (green line, *in situ* generated enamine) and the mixture of all the reagents (red line). [**1a**] = 1.5 M: 27.0 µL dissolved in 200 µL of MTBE; [**5**] = 0.5 M: 16.2 mg dissolved in 200 µL of MTBE; [*(R)*-**A**] = 0.1 M: 11.9 mg dissolved in 200 µL of MTBE. **1a** + **A**: solution of 27.0 µL of **1a** and 11.9 mg of **A** in 200 µL of MTBE. Mixture of all the reagents: solution of 27.0 µL of **1a**, 11.9 mg of **A** and 18.2 mg of **5** in 200 µL of MTBE.

When mixing together the enamine, generated *in situ* upon condensation of catalyst **A** and **1a** (green line in Figure S5), with 2,4-dinitrotoluene **5**, the optical absorption spectra showed a bathochromic displacement in the visible spectral region, where none of the substrates absorbs (red lines, Figure S5). The new absorption band indicates the formation of an EDA complex.

C2. EDA Complex Formation with the Preformed Enamine 4

The preformed enamine **4**, prepared according to the literature (*2*), was mixed with the EDA acceptors **2a**, **2b** and **5**. The absorption spectra of the resulting mixtures showed the formation of new absorption bands diagnostic of EDA complex formation (red lines in Figure S6).

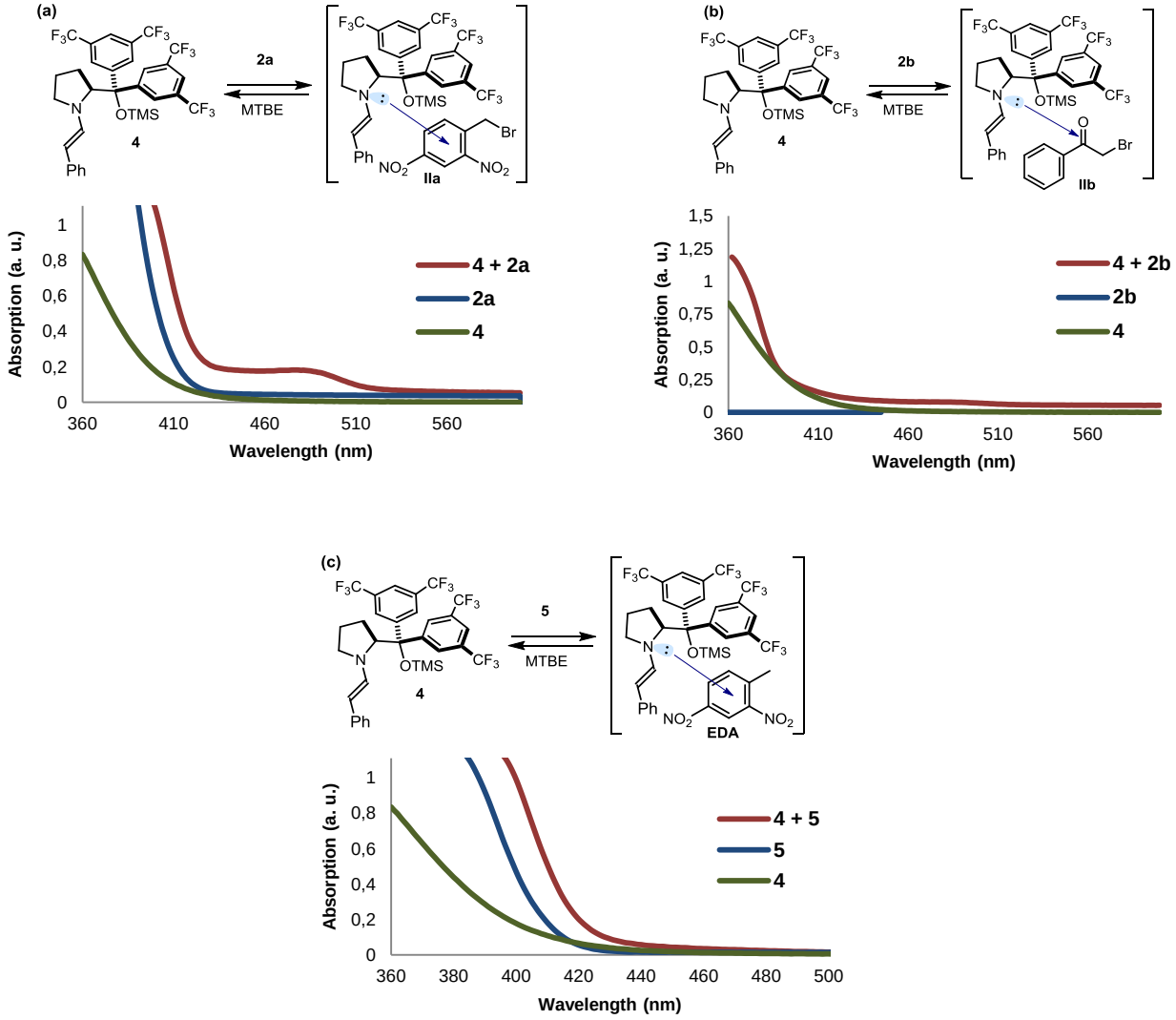

Figure S6. Absorption spectra of the mixtures of enamine **4** (green line) with (**a**) 2,4-dinitrobenzylbromide **2a**, (**b**) phenacyl bromide **2b**, and (**c**) 2,4-dinitrotoluene **5**. [**4**] = 0.04 M in MTBE, prepared by diluting 1 mL of a 0.4 M solution of **4** in MTBE into 10 mL. [**2a**] = 0.5 M: 26 mg dissolved in 200 µL of MTBE; [**2b**] = 0.5 M: 20 mg dissolved in 200 µL of MTBE; [**5**] = 0.5 M: 18.2 mg dissolved in 200 µL of MTBE; **4** + **2a**: 26 mg of **2a** dissolved in 200 µL of a 0.04 M solution of **4**; **4** + **2b**: 20 mg of **2b** dissolved in 200 µL of a 0.04 M solution of **4**; **4** + **5**: 18.2 mg of **5** dissolved in 200 µL of a 0.04 M solution of **4**.

D. Characterization of EDA Complexes

D1. Stoichiometry of the EDA Complex in Solution

A Job's plot was constructed to evaluate the stoichiometry of the EDA complex (*6*) between 2,4-dinitrobenzylbromide (**2a**) and the preformed enamine **4**. We measured the absorption at 470 nm of MTBE solutions with different donor/acceptor ratios but constant concentration (0.1 M) of the two components. All the absorption spectra were recorded in 1 mm path quartz cuvettes using a Shimadzu 2401PC UV-visible spectrophotometer. The absorbance values are plotted against the molar fraction (%) of 2,4-dinitrobenzyl bromide. The maximum absorbance is obtained with a 1:1 mixture, indicating that this is the stoichiometry of the EDA complex in solution. The same procedure was repeated to evaluate the stoichiometry in solution of the EDA complex between enamine **4** and bromoacetophenone (**2b**), obtaining identical results.

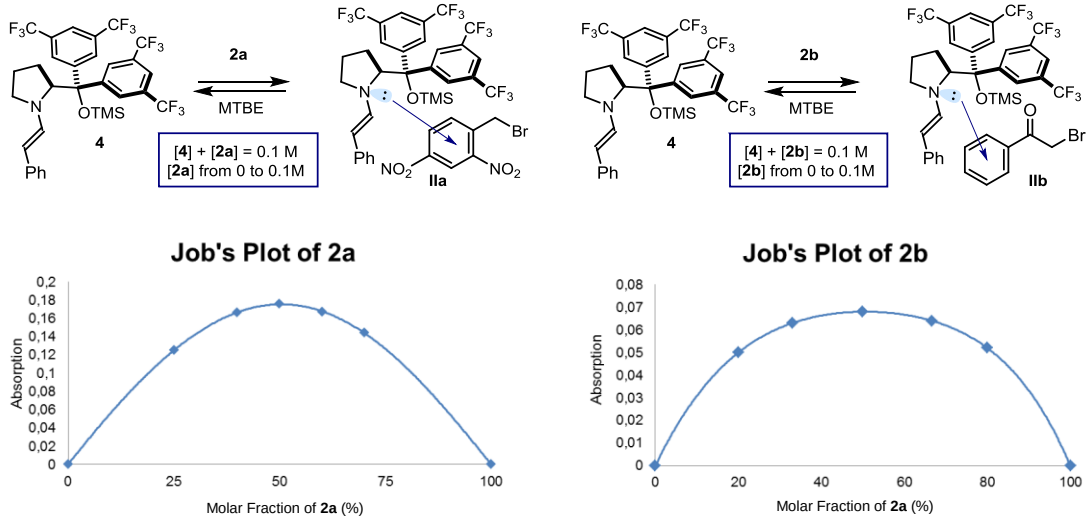

Figure S7. Job's plots of the EDA complexes **IIa** and **IIb** in MTBE.

D2. Determination of the Association Constant (K_{EDA})

The association constant of the EDA complex formed between 2,4-dinitrobenzylbromide (**2a**) and enamine **4** was determined spectrophotometrically in MTBE, employing the Hildebrand-Benesi methodology (*7*). We measured the absorption at 470 nm of solutions with constant concentration of the enamine **4** (0.04 M) but increased donor/acceptor ratio, adding an excess of the benzyl bromide **2a**. All the absorption spectra were recorded in 1 mm path quartz cuvettes using a Shimadzu 2401PC UV-visible spectrophotometer. According to the methodology, a straight line is obtained when the reciprocal of the absorbance (A) is plotted against the reciprocal of the concentration of the partner in excess. The procedure was repeated to determine the association constants of the EDA complexes formed by mixing the enamine **4** with the acceptors **2b**, and **5**. The plots, obtained for the calculation of the association constants of **2a**, **2b** and **5** with the preformed enamine **4**, are displayed below. The following association constants (K_{EDA}), calculated dividing the intercept by the slope, were determined: **11.56 ± 0.02 M^{-1}** for the **2a**/**4** complex; **4.9 ± 0.1 M^{-1}** for the for the **2b**/**4** complex; and **4.6 ± 0.1 M^{-1}** for the for the **5**/**4** complex.

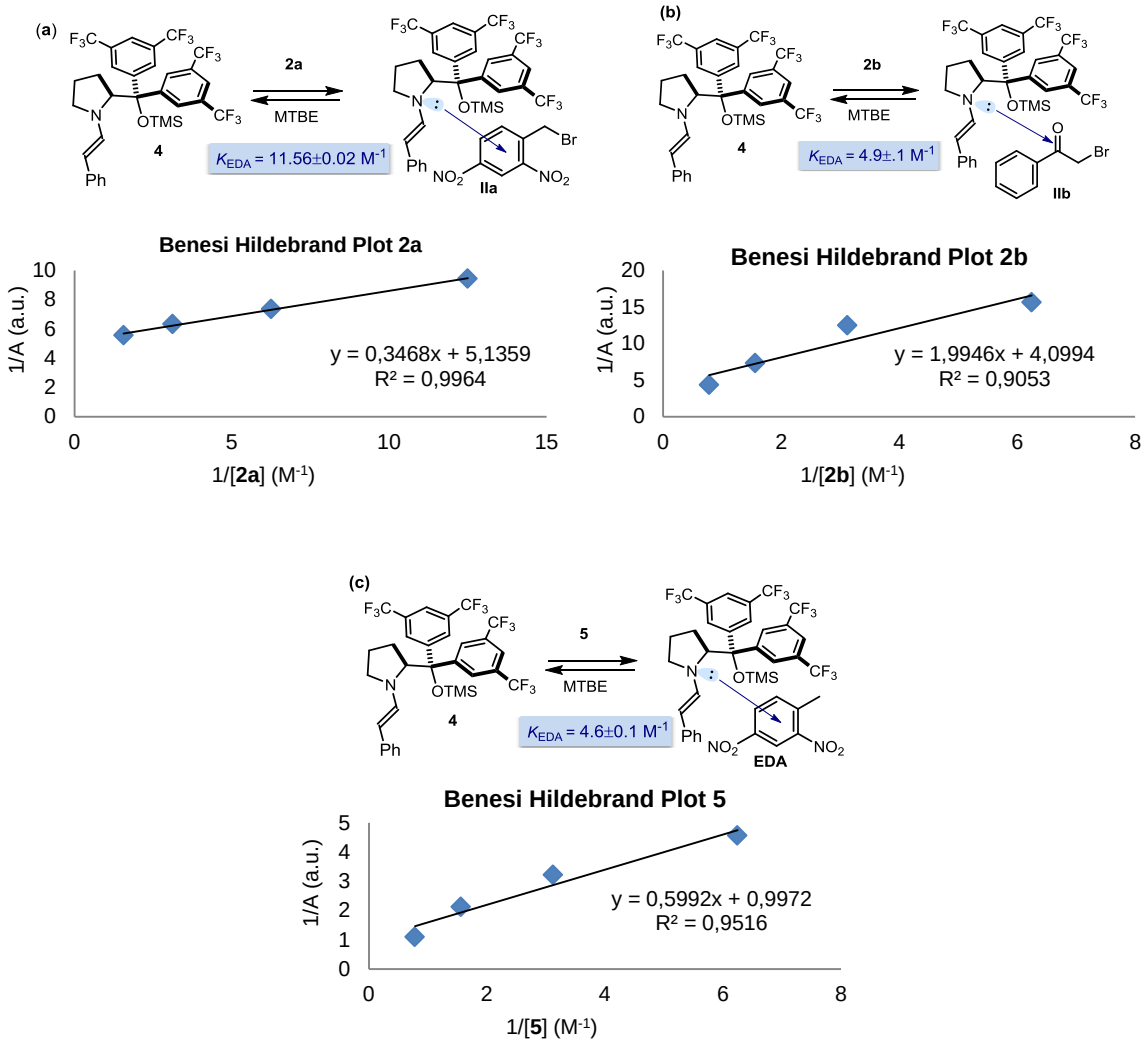

Figure S8. Hildebrand-Benesi plots for the EDA complexes generated in MTBE upon association of the enamine **4** and (**a**) 2,4-dinitrobenzylbromide **2a**, (**b**) phenacyl bromide **2b**, and (**c**) 2,4-dinitrotoluene **5**.

E. Mechanistic Studies on the Direct Photoexcitation of Enamines

E1. Absorption and Emission Spectrum of the Preformed Enamine 4

E1a. UV-vis absorption spectrum of the enamine **4**

Procedure for the acquisition of absorption spectra: Solutions at different concentrations of the enamine **4** (obtained by opportunely diluting the original stock solution with dry toluene) were introduced to a 1 cm path length quartz cuvette equipped with a Teflon® septum under an argon atmosphere and analyzed using a spectrophotometer.
The absorbance shows a typical Lambert-Beer linear correlation with the concentration at different wavelengths.

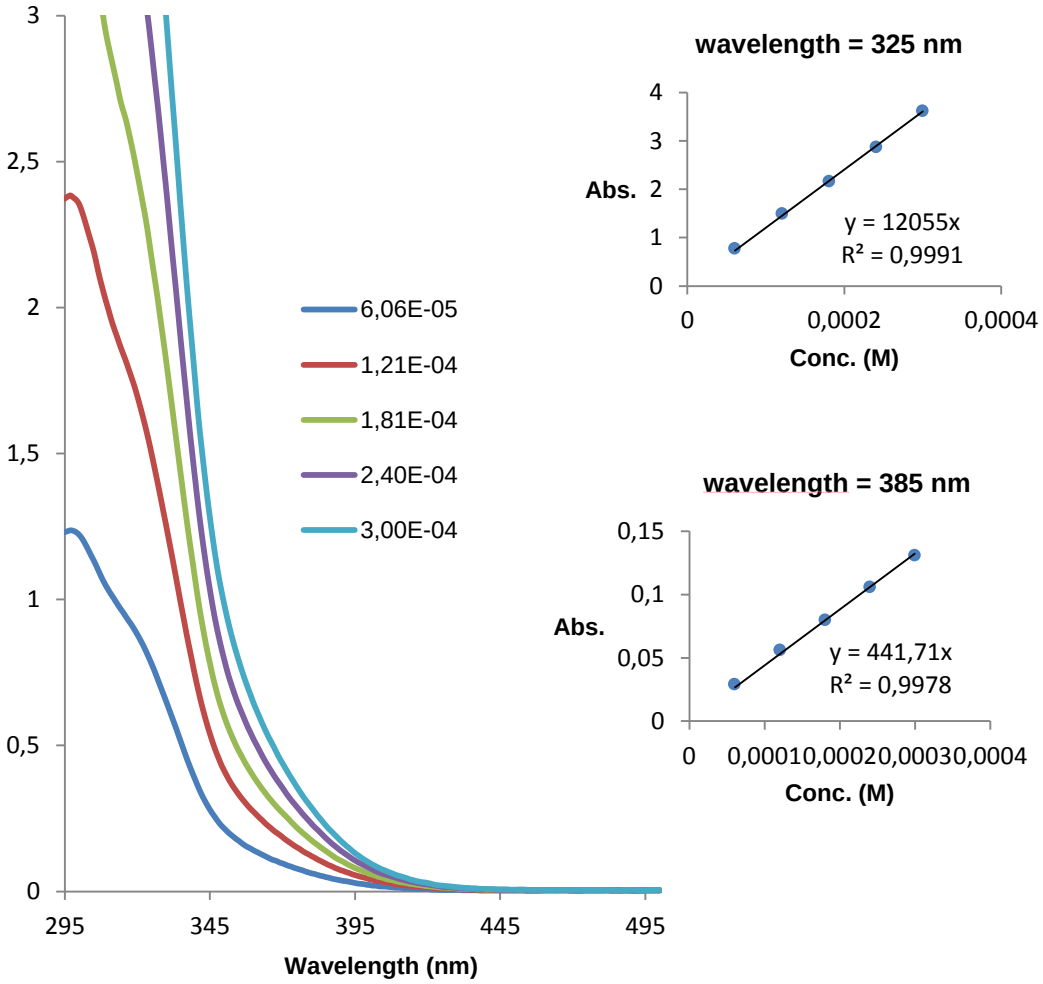

Figure S9. Absorption spectra of the enamine **4** at different concentrations in toluene.

E1b. Emission Spectrum of the Preformed Enamine **4**

The emission spectra were recorded in a Fluorolog Horiba Jobin Yvon spectrofluorimeter equipped with photomultiplier detector, double monochromator and 350 W xenon light source. A 2 mL of a $5 \cdot 10^{-5}$ M solution (dry toluene) of the enamine **4** was placed in a 10 x 10 mm light path quartz fluorescence cuvette equipped with Silicone/PTFE 3.2 mm septum under an argon atmosphere. The excitation wavelength was fixed at 365 nm (incident light slit regulated to 1 mm), while the emission light was acquired from 400 nm to 750 nm (emission light slit regulated to 15 mm). A solvent blank was subtracted from the measurement.
The regulation of the excitation light slit width was crucial for the experiment in order to avoid the occurrence of an undesired photochemical process (double bond isomerization) of the enamine, resulting in detectable spectral variations (both emission and absorption). Under the conditions described above, the undesired isomerization process was not detected.

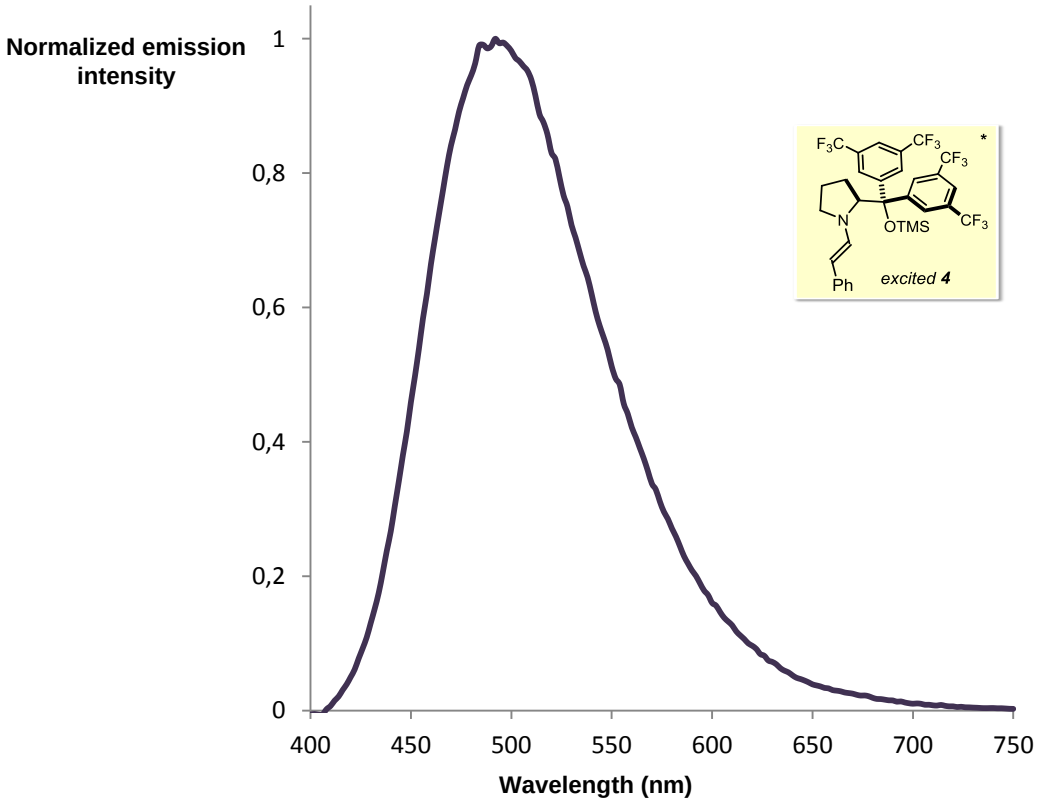

Figure S10. Emission spectrum of the enamine **4** (excitation wavelength 365 nm).

E2. Stern-Volmer Quenching Studies with Bromomalonate 2c

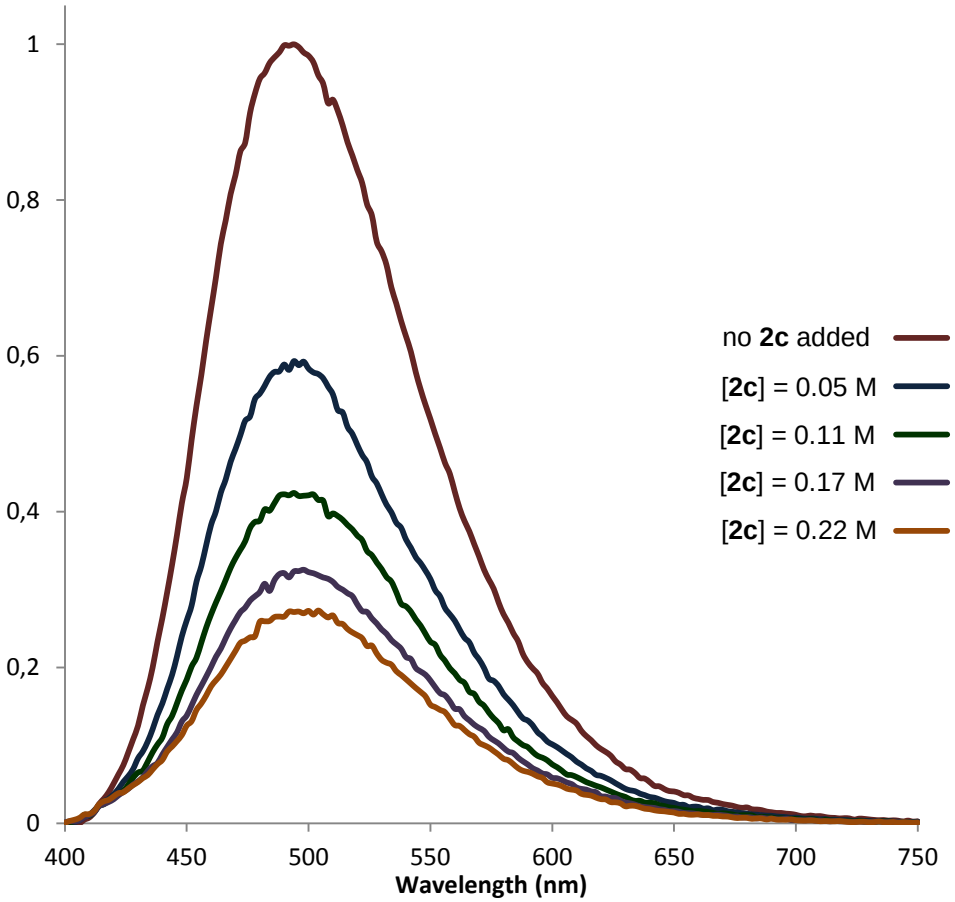

Figure S11. Quenching of the enamine **4** emission ($5 \cdot 10^{-5}$ M in toluene) in the presence of increasing amounts of bromomalonate **2c.**

The samples were prepared mixing the enamine **4** ([**4**] = $5 \cdot 10^{-5}$ M) with the required amount of **2c** in a total volume of 2 mL of dry toluene in a 10x10 mm light path quartz fluorescence cuvette equipped with Silicone/PTFE 3.2 mm septum under an argon atmosphere. The samples were vigorously bubbled with dry argon for 5 minutes prior to the measurement. The excitation wavelength was fixed at 365 nm (incident light slit regulated to 1 mm), the emission light was acquired from 400 nm to 750 nm (emission light slit regulated to 15 mm). A solvent blank was subtracted from all the measurements.
The excitation wavelength was chosen in order to avoid *inner-filter* effect due to the absorption of **2c**.

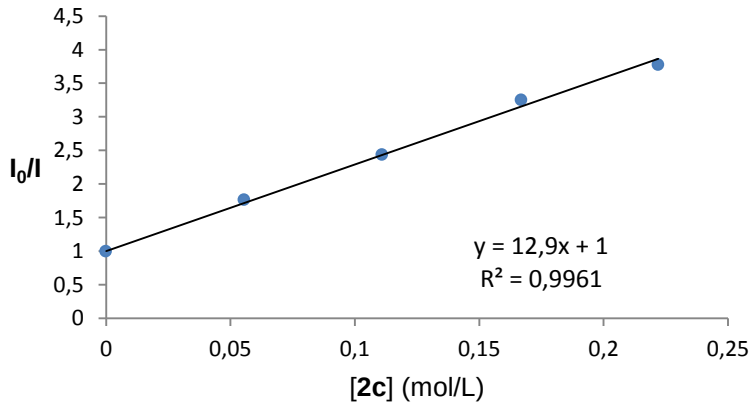

Figure S12. Stern-Volmer quenching plot.

The Stern-Volmer plot shows a linear correlation between the amounts of **2c** and the ratio I_0/I. On the basis of the following Equation S1, it is possible to calculate the Stern-Volmer constant K_{SV} (*8*).

$$I_0/I = 1 + K_{SV}[Q] \qquad \text{Eq. S1}$$

We calculated a Stern-Volmer quenching constant of **12.9 M^{-1}**.

A static quenching can occur if a complex is formed in the ground state between the enamine **4** and **2c**. In order to rule out this possibility, a careful analysis of the absorption spectra of the enamine **4** in the presence of increasing amounts of **2c** (the same amount and concentrations have been used as in the emission quenching studies) has been carried out. The sample for the analysis was prepared in the same way as for the emission quenching experiments.

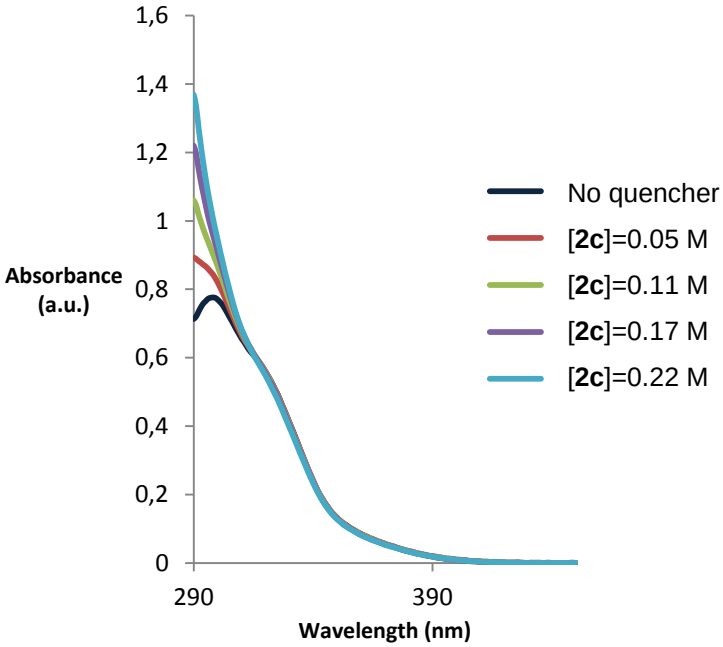

Figure S13. Absorption spectra of the enamine **4** in the presence of increasing amounts of **2c**.

No spectral variations were observed in the area between 330 nm – 450 nm, further excluding any EDA association in the ground state.

In order to verify that the spectral variations observed at lower wavelength (< 320 nm) are due to the additive absorbance of **2c**, spectroscopic analysis were carried out on **2c** at the concentration employed for the quenching study. These studies, detailed in Figure S14, confirmed the additive absorbance of **2c** at lower wavelength.

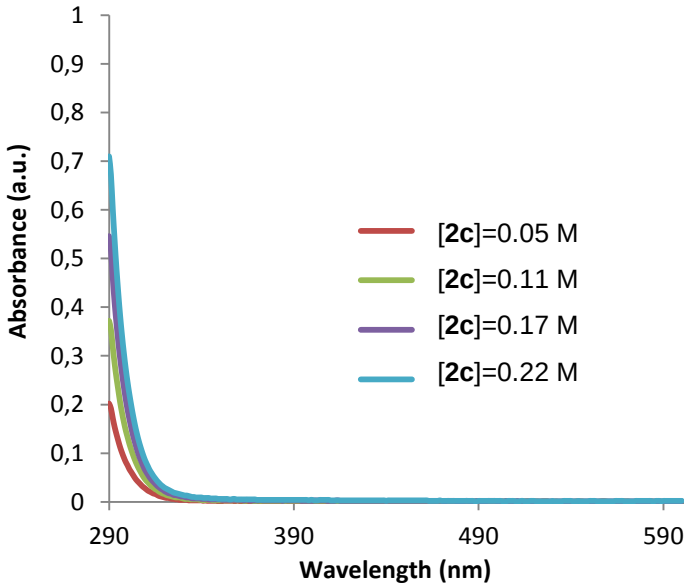

Figure S14. Absorption spectra of **2c** at different concentrations.

Collectively, our investigations, including the linear Stern-Volmer plot and the absorption spectra studies, are indicative of a dynamic quenching and of an interaction between the enamine **4** in the excited state and the ground state of bromomalonate **2c**.

Effect of the oxygen on the enamine 4 emission:

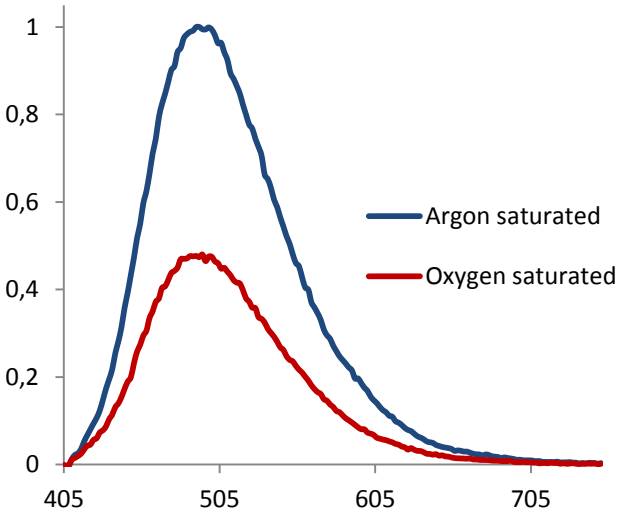

Figure S15. Effect of oxygen on the emission spectra of **4**.

Procedure for the control experiment of emission quenching by oxygen:
The samples were prepared mixing the enamine **4** (conc. $5 \cdot 10^{-5}$ M) in a total volume of 2 mL of dry toluene. The samples were vigorously bubbled with dry argon (or dry oxygen) for 5 minutes prior to the measurement. For the experiment, a Silicone/PTFE 3.2 mm septum equipped fluorescence quartz cuvette was employed. A solvent blank was subtracted from all the measurements.

This study confirms that oxygen is an active quencher for the excited state of enamine **4**, which is consonant with the sensitivity of the photoorganocatalytic reactions with bromomalonate **2c** to the presence of oxygen.

E3. Electrochemical Analysis of the Preformed Enamine 4

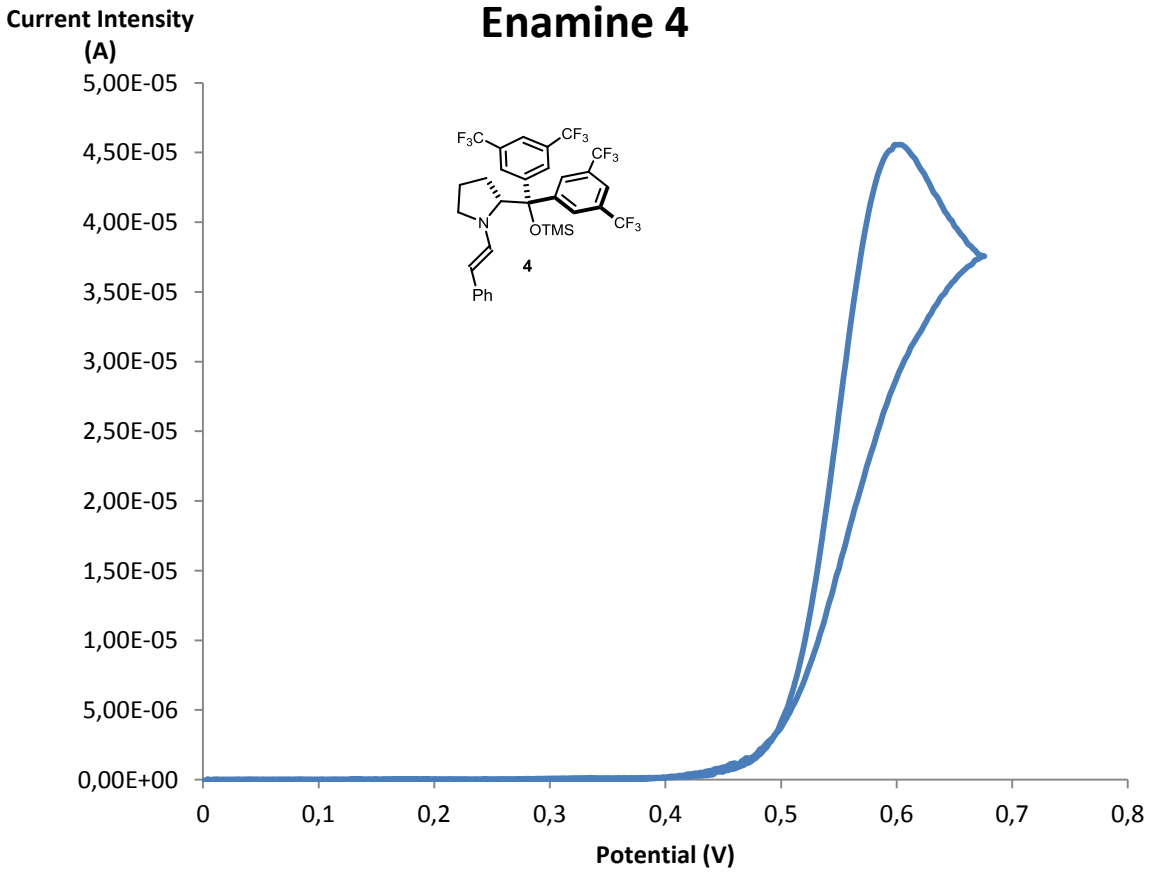

Figure S16. Cyclic voltammetry carried out on preformed enamine **4**.

Electrochemical grade tetrabutylammonium hexafluorophosphate (116 mg, 0.300 mmol) was added to a 0.01 M solution of enamine **4** in 3 mL of dry acetonitrile and the solution was vigorously bubbled with N_2 for 5 minutes prior to the measurement. The oxidation potential was measured using a glassy carbon working electrode, a platinum wire counter electrode, and a NaCl saturated Ag/AgCl reference electrode at 5 mV/s scan rate.
A completely irreversible oxidation wave was observed with $E_P^A = 0.60$ V.
The cyclic voltammetry of the individual catalyst **A** and phenylacetaldehyde was also carried out, using the same experimental conditions and concentrations. As expected, no oxidation waves were

detected for phenylacetaldehyde in the range 0 – 1.5 V, while the cyclic voltammetry curve of the catalyst is reported below.

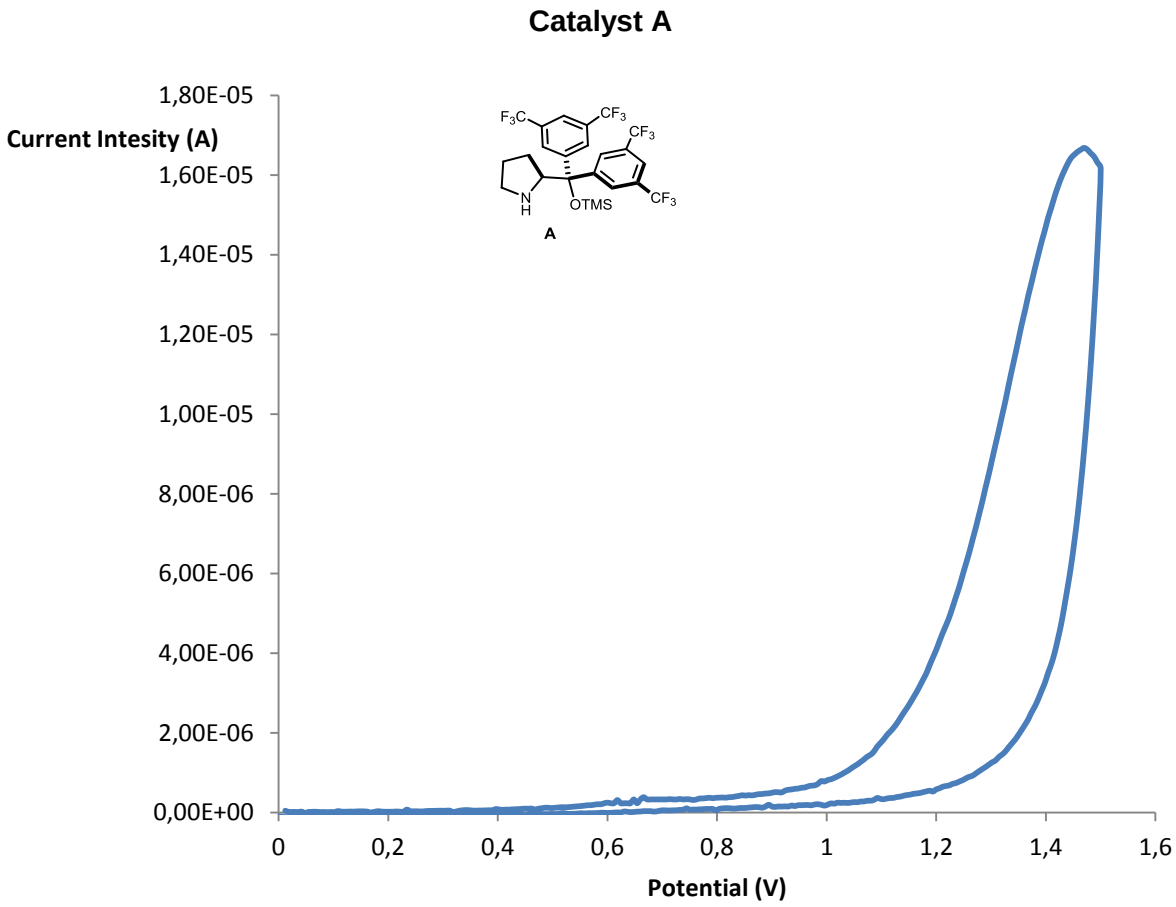

Figure S17. Cyclic voltammetry of the catalyst **A**.

Using this data, we estimated the redox potential of the excited enamine **4** employing the following Equation S2 (Ref. *9*):

$$E(\mathbf{4}^{\cdot+}/\mathbf{4}^{*}) = E(\mathbf{4}^{\cdot+}/\mathbf{4}) - E_{0\text{-}0}(^{*}\mathbf{4}/\mathbf{4}) \qquad \text{Eq. S2}$$

(note that $\mathbf{4}^{\cdot+}$ is the the α-iminyl radical cation **V** in the main manuscript)

Since the electrochemical oxidation of the enamine **4** was totally irreversible, the irreversible peak potential E_P^A was used for $E(\mathbf{4}^{\cdot+}/\mathbf{4})$. $E_{0\text{-}0}(^{*}\mathbf{4}/\mathbf{4})$, the excited state energy of the enamine **4**, was estimated spectroscopically from the position of the long wavelength tail of the absorption spectrum (Figure S18) recorded in the acetonitrile, the solvent used for the electrochemical analysis, according to (*10*). This corresponds to 420 nm, which translates into an $E_{0\text{-}0}(^{*}\mathbf{4}/\mathbf{4})$ of 2.95 eV for the enamine.

$$E(\mathbf{4}^{\cdot+}/\mathbf{4}^{*}) = 0.60 - 2.95 = -2.35 \text{ V (vs Ag/AgCl)}$$

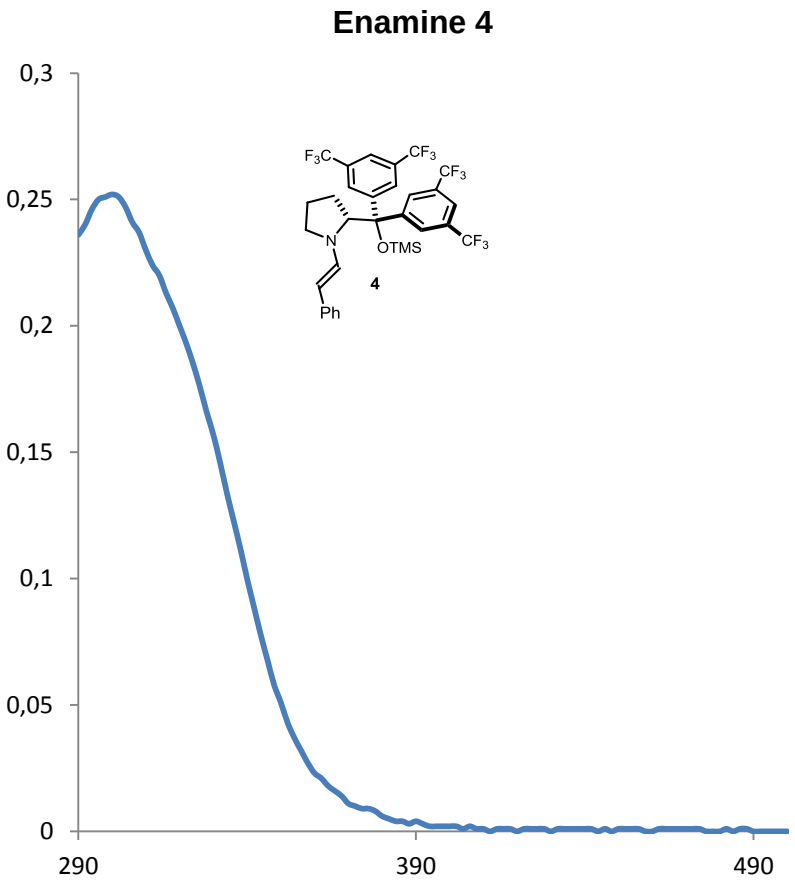

Figure S18. Absorption spectrum of a $2 \cdot 10^{-5}$ M solution of enamine **4** in dry acetonitrile, the tail wavelength was considered to be at about 420 nm.

F. Studies on the Catalyst Degradation

F1. Evolution of the catalyst concentration over time

The evolution of the catalyst **A** concentration under the optimal reaction conditions, depicted in Scheme S1, has been studied.

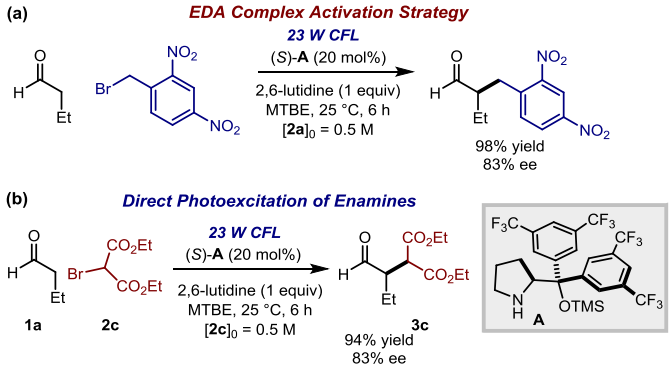

Scheme S1. The model reactions.

A GC-FID was calibrated to correlate the signal of the catalyst **A** versus the signal obtained for 1,3,5-trimethoxybenzene, which was used as the internal standard (**IS**). The calibration curve is depicted in Figure S19.

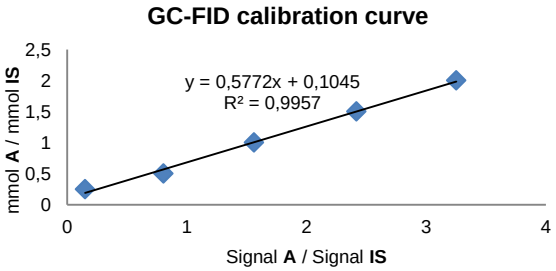

Figure S19. GC-FID calibration curve for different catalyst (**A**) to 1,3,5-trimethoxybenzene (**IS**) ratios.

For the two different photochemical alkylations in Scheme S1, three identical reactions were set up in Schlenk tubes after careful de-oxygenation of the reaction medium, and quenched after 2, 4, and 6 hours. The reactions were performed according to the general procedure describe in page S4.

For the EDA-based system (Scheme S1a), a stock solution containing 47.6 mg of **A** (0.08 mmol) and 13.6 mg of 1,3,5-trimethoxybenzene (0.08 mmol) in 800 μL of MTBE was prepared. Each Schlenk tube was filled with 200 μL of the stock solution, 27 μL of **1a** (0.3 mmol, 3 eq), 12 μL of 2,6-lutidine (0.1 mmol, 1 eq) and 26 mg of **2a** (0.1 mmol, 1 eq). The solutions were thoroughly degassed with three cycles of freeze-pump-thaw and then placed 4 cm away from a 23 W CFL bulb.

For the alkylation with bromomalonate **2c** (Scheme S1b), the same procedure was carried out. An equivalent stock solution was prepared, each Schlenk tube was filled with 200 μL of the stock solution, 27 μL of **1a** (0.3 mmol, 3 eq), 12 μL of 2,6-lutidine (0.1 mmol, 1 eq) and 17 μL of **2c** (0.1 mmol, 1 eq). The solutions were thoroughly degassed with three cycles of freeze-pump-thaw and then placed 4 cm away from a 23 W CFL bulb.

The reactions were stopped after irradiating for 2, 4 or 6 hours and the amount of catalyst present was monitored by GC-FID. As shown in Table S1, the catalyst **A** degradation is more pronounced in the EDA complex-mediated alkylation with **2a**. For the α-alkylation of aldehydes with bromomalonate **2c**, a much slower degradation is observed.

Table S1. Evolution of the catalyst **A** concentration and the product **3** formation over time.

Entry	Alkyl halide	time (h)	Yield of **3**[a]	Catalyst **A** remaining[b]
1	**2a**	2	**3a**, 36%	76%
2	**2a**	4	**3a**, 75%	40%
3	**2a**	6	**3a**, >95%	31%
4	**2c**	2	**3c**, 45%	85%
5	**2c**	4	**3c**, >95%	79%
6	**2c**	6	**3c**, >95%	78%

[a] NMR yield of **3** determined by ^{1}H NMR spectroscopic analysis of the crude reaction mixture. [b] Yield of the remaining catalyst **A** measured by GC-FID.

F2. Evolution of the catalyst concentration in solution irradiating with monochromatic light

A more thorough investigation of the evolution of the catalyst **A** over time was carried out measuring the catalyst degradation irradiating with a more stable light source. We used a 300 W xenon lamp coupled with a band pass filter at 450 nm. A series of experiments were performed in identical Schlenk tubes quenched at different conversions (all below 20% of conversion). These experiments were carried out with different initial concentrations of **2a** or **2c** and using NMR analysis to monitor the amount of catalyst in solution.

EDA-based system using **2a** (Figure S20):

Sets of three reactions with equivalent concentrations of every reactant except for **2a** were carried out in three identical Schlenk tubes. The Schlenk tubes containing the degassed reaction mixtures were positioned 10 cm away from the light source. They were irradiated with 300 W Xenon Lamp operating at 100% of light intensity with a bandpass filter of 450 ± 5 nm without stirring (irradiance: 4.7 mW/cm^2). This procedure was repeated 4 times, quenching the reactions after different time intervals.

The model reaction was set up utilizing a stock solution containing 360 mg of the aminocatalyst **A** (0.6 mmol) and 15 mg of 1,3,5-trimethoxybenzene (employed as internal standard to measure the conversion of the enamine in solution) dissolved in 6 mL of CD_3CN. Butyraldehyde **1a** (54 μL, 0.6 mmol, 3 equiv.) was added to 400 μL of this solution, followed by the addition of 24 μL of 2,6-lutidine (0.2 mmol, 1 equiv.) and 54 mg of 2,4-dinitrobenzyl bromide **2a** (0.2 mmol, 1 equiv.). The reaction mixtures were degassed via freeze pump thaw (x 3 cycles), and the vessel refilled with argon. After irradiating for the indicated time, the conversion of 2,4-dinitrobenzyl bromide **2a** was checked by ^{1}H NMR and the remaining catalyst in solution was calculated employing 1,3,5-trimethoxybenzene as internal standard by integration of the enamine peaks (under the reaction conditions, no free catalyst **A** could be detected). For this reaction, the concentrations are: [**A**] = 0.1 M, [**1a**] = 1.5 M, [**2a**] = [2,6-lutidine] = 0.5 M. Alongside with this reaction, other two identical solutions were prepared varying the concentration of the reagent **2a**: $[\mathbf{2a}]_0$ = 0.25 M and 1 M.

The experiments, performed irradiating with a Xenon lamp with a band-pass filter at 450 nm, confirmed that the catalyst concentration in solution decreases as the reaction proceeds. Furthermore, the decrease in [**A**] correlates with **2a** concentration (Figure S20).

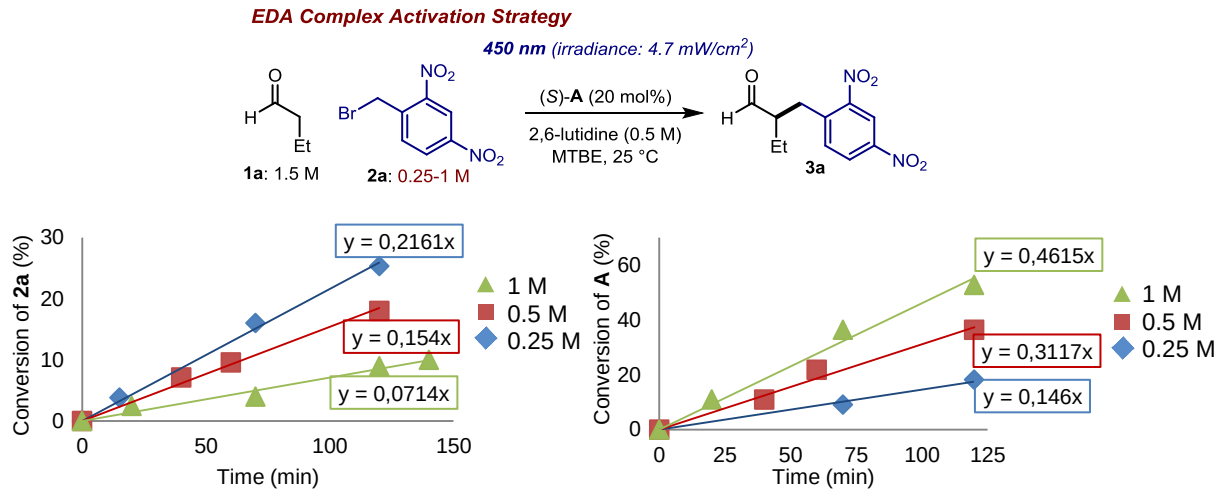

Figure S20. Reaction profiles for different [**2a**] (*left* panel) irradiating at 450 nm (irradiance 4.7 mW/cm^2): $[\mathbf{2a}]_0$ = 0.25 M (blue line), $[\mathbf{2a}]_0$ = 0.5 M (red line) and $[\mathbf{2a}]_0$ = 1 M (green line). Evolution of the catalyst concentration in solution for the same reactions (*right* panel). Since there is zero-order dependence in [**1a**] and due to the fact that we could not detect any trace of catalyst **A** in its free state by NMR analysis, we monitored the evolution of **A** in our experiments by determining the enamine concentration in solution.

α-alkylation of aldehydes with bromomalonate **2c**:

Equivalent experiments were carried out to study the evolution of the concentration of catalyst **A** in the alkylation of **1a** with **2c**. A 300 W Xenon lamp operating at 100% of light intensity and equipped with a cut-off filter at 385 nm ($\lambda \geq 385$ nm; irradiance = 300 mW/cm^2) was used to irradiate the reactions. In these experiments, conducted upon thorough de-oxygenation of the reaction medium, ***no significant*** degradation of catalyst **A** was observed below 20 % conversion.

F3. Evolution of the catalyst concentration in solution using *in situ* NMR monitoring

The reaction progress and the catalyst degradation were also followed using *in situ* monitoring by direct irradiation of non-degassed solutions. The reactions were run directly in the NMR tube, which precluded a thorough de-oxygenation of the reaction medium. For these experiments, we used a xenon lamp coupled with a monochromator which, by bringing the light in close contact with the NMR tube through an optical fiber, allowed for the *in situ* illumination of the samples. A larger rate of catalyst degradation was observed when the reaction was conducted in the presence of oxygen (degassing the reaction mixtures via freeze pump thaw was unviable).

The reactions were carried out employing a regular NMR tube as the reaction vessel. They were irradiated at 470 nm with a 150 W xenon high stability light lamp Tilluxe P45 coupled to a monochromator for exact wavelength definition. This polychromator is connected to an optical fiber that can be directly introduced into the NMR tube. This allowed us to monitor the reactions in real time with *in situ* irradiation inside the NMR spectrometer. The conversion of **2a** was checked by ^{1}H NMR and the concentration of the remaining catalyst **A** in solution was calculated employing 1,3,5-trimethoxybenzene as internal standard. Since there is zero-order dependence in [**1a**] and due to the fact that we could not detect any trace of catalyst **A** in its free state by NMR analysis, we monitored the evolution of **A** in our experiments by determining the enamine concentration.

The model reaction (Figure S21) was set up utilizing a stock solution containing 72 mg of the aminocatalyst **A** (0.12 mmol) and 3 mg of 1,3,5-trimethoxybenzene (employed as internal standard to measure the concentration of the enamine in solution) dissolved in 6 mL of CD_3CN, previously dried over 4 Å molecular sieves. Butyraldehyde **1a** (13.5 μL, 0.15 mmol, 3 equiv) was added to 500 μL of this solution, followed by the addition of 2,6-lutidine (6 μL, 0.05 mmol, 1 equiv), and 2,4-dinitrobenzyl bromide **2a** (13 mg, 0.05 mmol, 1 equiv). Resultantly, the concentrations utilized for the model reaction were: [**A**] = 0.02 M, [**1a**] = 0.3 M and [**2a**] = [2,6-lutidine] = 0.1 M. Alongside

with this reaction, other two identical solutions were prepared with a different concentration of **2a**: $[\mathbf{2a}]_0$ = 0.05 M and 0.2 M.

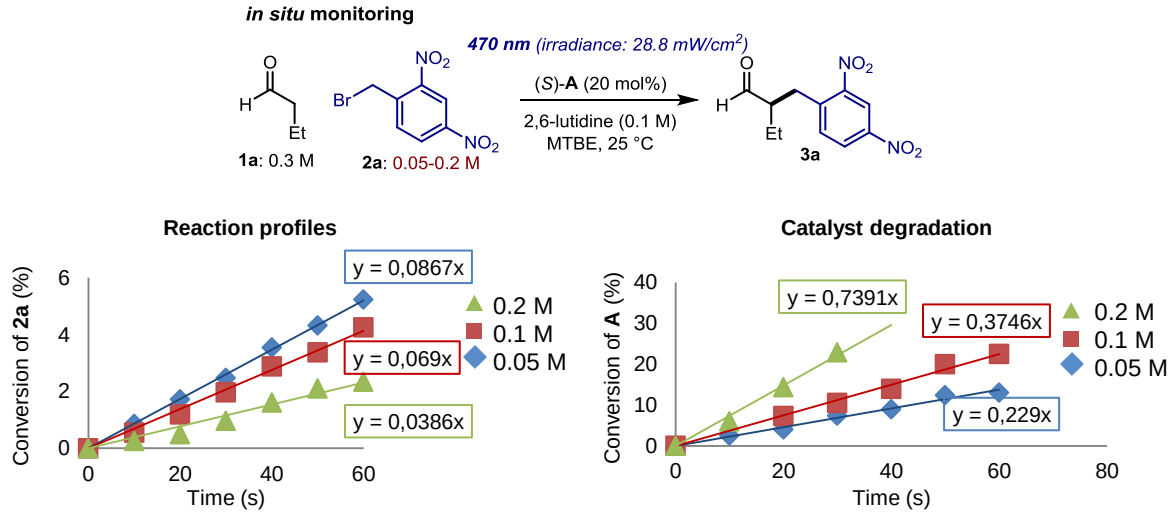

Figure S21. Reaction profiles for different [**2a**] (*left* panel) irradiating *in situ* at 470 nm (irradiance 28.8 mW/cm^2): $[\mathbf{2a}]_0$ = 0.05 M (blue line), $[\mathbf{2a}]_0$ = 0.1 M (red line) and $[\mathbf{2a}]_0$ = 0.2 M (green line). Evolution of the catalyst concentration in solution for the same reactions (*right* panel). Since there is zero-order dependence in [**1a**] and due to the fact that we could not detect any trace of catalyst **A** in its free state by NMR analysis, we monitored the evolution of **A** in our experiments by determining the enamine concentration in solution.

Using the *in situ* monitoring of the processes, we confirmed that the catalyst concentration in solution decreases as the reaction proceeds. Furthermore, the decrease in [**A**] correlates with **2a** concentration.

The same experiments as in Figure S21 were repeated using a different intensity of irradiation (λ = 470 nm, but irradiance = 3.0 instead of 28.8 mW/cm^2). In the latter set of experiments, detailed in Figure S22, a lower absolute rate of catalyst disappearance was determined, in consonance with a less effective initiation regime. This observation establishes a direct correlation between the disappearance of catalyst **A** and the number of photochemical initiation events, since both the concentration of **2a** and the intensity of light influence the rate of degradation for catalyst **A**.

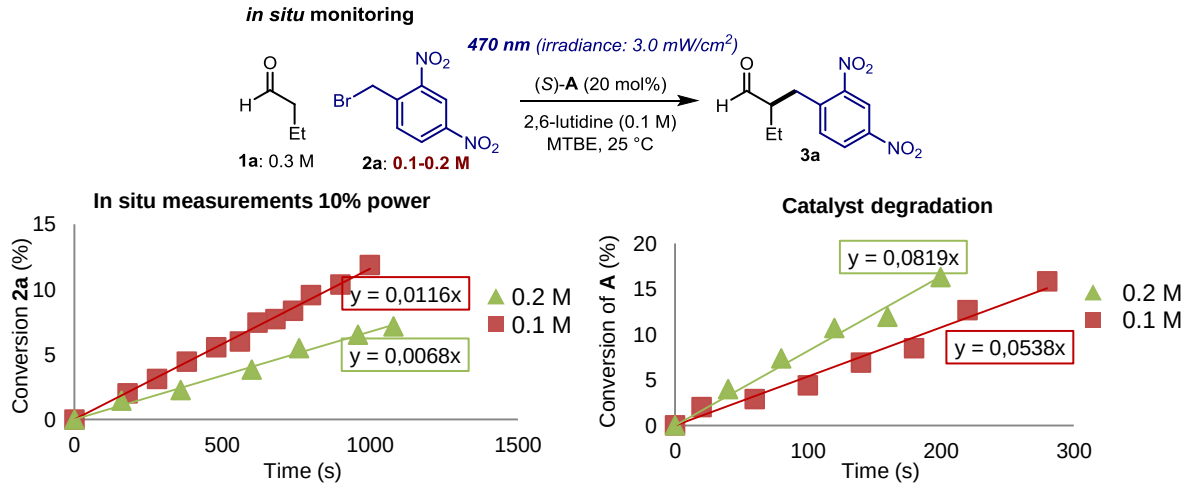

Figure S22. Reaction profiles for different [**2a**] (*left* panel) irradiating *in situ* at 470 nm (irradiance 3.0 mW/cm^2): $[\mathbf{2a}]_0$ = 0.1 M (red line) and $[\mathbf{2a}]_0$ = 0.2 M (green line). Evolution of the catalyst concentration in solution for the same reactions (*right* panel).

α-alkylation of aldehydes with bromomalonate **2c**:
Equivalent experiments, using *in situ* irradiation, were carried out to study the evolution of the concentration of catalyst **A** in the reaction with **2c**. When irradiating at λ = 400 nm (irradiance = 20.4 mW/cm^2), we *did observe catalyst degradation* (after 150 seconds of reaction, 5% yield of product **3c** and 97% of catalyst **A** remaining; after 350 seconds of reaction, 10% yield of product **3c** and 45% of catalyst **A** remaining).
This is presumably because of decomposition pathways triggered by the presence of oxygen in the system, as *in situ* monitoring did not allow for complete de-oxygenation of the reaction medium.

G. Quantum Yield Measurements

G1. Quantum Yield Measurement for the EDA complex-mediated reactions

A ferrioxalate actinometer solution was prepared by following the Hammond variation of the Hatchard and Parker procedure outlined in *Handbook of Photochemistry (11).* The ferrioxalate actinometer solution measures the decomposition of ferric ions to ferrous ions, which are complexed by 1,10-phenanthroline and monitored by UV/Vis absorbance at 510 nm. The moles of iron-phenanthroline complex formed are related to moles of photons absorbed.

The solutions were prepared and stored in a dark laboratory (red light):

1. Potassium ferrioxalate solution: 589.5 mg of potassium ferrioxalate (commercially available from Alfa Aesar) and 278 μL of sulfuric acid (96%) were added to a 100 mL volumetric flask, and filled to the mark with water (HPLC grade).
2. Phenantroline solution: 0.2% by weight of 1,10-phenanthroline in water (200 mg in 100 mL volumetric flask).
3. Buffer solution: to a 100 mL volumetric flask, 4.94 g of NaOAc and 1 mL of sulfuric acid (96%) were added and filled to the mark with water (HPLC grade).
4. Model reaction solution: a stock solution containing 300 mg of the aminocatalyst **A** (0.5 mmol), and 300 μL of 2,6-lutidine (2.5 mmol) were added to a 5 mL volumetric flask and filled to the mark with acetonitrile (HPLC grade). To 1 mL of this solution, butyraldehyde **1a** (135 μL, 1.5 mmol, 3 equiv.) and 2,4-dinitrobenzyl bromide **2a** (130 mg, 0.5 mmol, 1 equiv.) were sequentially added. The mixture was kept in the dark for 20 minutes (1 hour in the case of the bromoacetophenone **2b**) in order to reach a constant amount of EDA in solution. Concomitantly, 1 mL of this mixture was degassed and used to run the experiment.

Procedure: 1 mL of the actinometer solution and 1 mL of the degassed model reaction (alkylation of **1a** with **2a** or **2b**), whose quantum yield is being measured, were added to two identical quartz cuvettes (l = 10 mm). The cuvettes were placed 10 cm away from the light source. They were irradiated together with a 300 W Xenon Lamp operating at 50% of light intensity with a bandpass filter of 450 ± 5 nm without stirring. This procedure was repeated 4 times, quenching the reactions after different time intervals: 10, 12.5, 15, and 17.5 minutes.

The actinometer measurements were done as follows:

1. After irradiation, the actinometer solution was removed and placed in a 10 mL volumetric flask containing 0.5 mL of 1,10-phenanthroline solution and 2 mL of buffer solution. This flask was filled to the mark with water (HPLC grade).
2. The UV-Vis spectra of the complexed actinometer samples were recorded for each time interval. The absorbance of the complexed actinometer solution was monitored at 510 nm.

The moles of Fe^{2+} formed for each sample are determined according to the Beer's Law (Eq. S3):

$$moles\ Fe^{+2} = \frac{V_1 \cdot V_3 \cdot \Delta A(510\ nm)}{10^3 \cdot V_2 \cdot l \cdot \varepsilon(510\ nm)} \text{ (Eq. S3)}$$

where V_1 is the irradiated volume (1 mL), V_2 is the aliquot of the irradiated solution taken for the determination of the ferrous ions (1 mL), V_3 is the final volume after complexation with phenanthroline (10 mL), *l* is the optical path-length of the irradiation cell (1 cm), ΔA(510 nm) the optical difference in absorbance between the irradiated solution and the one stored in the dark, ε(510 nm) is that of the complex $Fe(phen)_3^{2+}$ (11100 L mol^{-1} cm^1).
The moles of Fe^{2+} formed (x) are plotted as a function of time (t). The slope of this line was correlated to the moles of incident photons by unit of time ($q^0_{n,p}$) by the use of the following Equation S4 (*12*):

$$\Phi(\lambda) = \frac{dx/dt}{q^0_{n,p}[1-10^{-A(\lambda)}]} \quad \text{(Eq. S4)}$$

where dx/dt is the rate of change of a measurable quantity (spectral or any other property), the quantum yield (Φ) for Fe^{2+} at 450 nm is 0.9 (*13*), and *A*(λ) is the absorbance of the actinometer at the wavelength used to carry out the experiments (450 nm). The absorbance at 450 nm *A*(450) was measure using a Shimadzu 2401PC UV-Vis spectrophotometer in 1 mm path quartz cuvettes in the presence of the bandpass filter of 450 nm employed to run the measurements, obtaining an absorbance of 0.156.
$q^0_{n,p}$, which is the photon flux, was determined to be $1.18 \cdot 10^{-9}$ einstein s^{-1}.

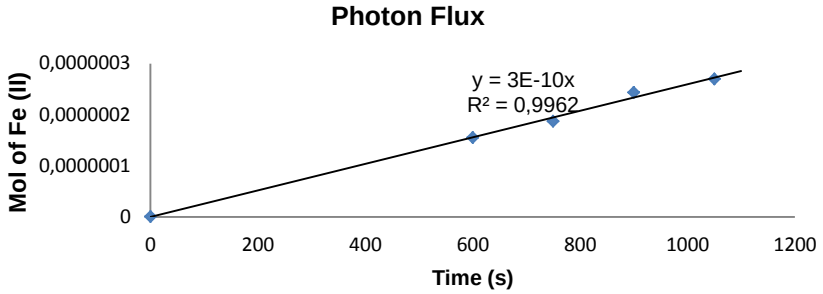

The measurements for the reaction under study were done as follows:
The moles of product **3** formed were determined by GC measurement (FID detector) using 2,4-dinitrotoluene as internal standard when using **2a** as the substrate. 1,3,5-trimethoxybenzene was used instead when the alkylation was performed with bromoacetophenone **2b**. The moles of product per unit of time are related to the number of photons absorbed. The photons absorbed are correlated to the number of incident photons by the use of the equation displayed in the previous point. According to Equation S4, if we plot the moles of product (x) versus the moles of incident photons ($q^0_{n,p} \cdot dt$), the slope is equal to: $\mathbf{\Phi \cdot (1\text{-}10^{-A(450\ nm)})}$, where Φ is the quantum yield to be determined and *A*(450 nm) is the absorption of the reaction under study. *A*(450 nm) was measured using a Shimadzu 2401PC UV-Vis spectrophotometer in 1 mm path quartz in the presence of the bandpass filter of 450 nm employed to carry out the measurements. An absorbance of 1.05 was determined for the reaction with **2a**.

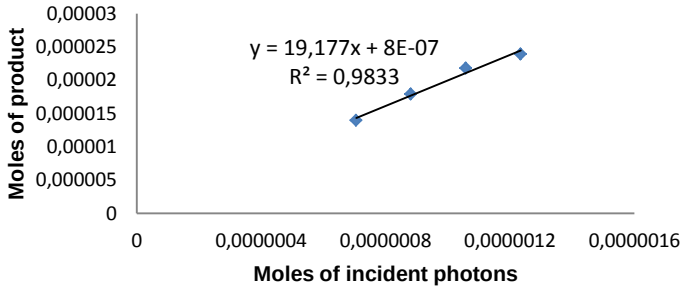

The quantum yield (Φ) of the photochemical alkylation of butanal **1a** with 2,4-dinitrobenzylbromide **2a** catalyzed by **A** was calculated to be **26**. The procedure was repeated a second time to provide a similar value: quantum yield (Φ) at 450 nm of **24**.

Using the same procedure, we calculated the quantum yield of the photochemical alkylation of butanal **1a** with bromoacetophenone **2b**. In this case, quantum yields of **19** and **20** were obtained in two independent experiments.

G2. Quantum Yield of the Initiation Step for the EDA complex-mediated reactions.
Using the procedure described in the previous section, the quantum yield of the initiation step was measured to better estimate the effective chain length. This has been done by monitoring the decomposition of the catalyst **A**. The analysis is based on the observation that the enamine **I**, generated upon condensation of catalyst **A** and butanal **1a**, serves as a sacrificial initiator of the chain mechanism since, for any photoinduced SET event, a propagating radical **IV** is generated while a molecule of the chiral catalyst **A** is destroyed via decomposition of the intermediate **V** (see Section F). Thus, any photo-induced initiation consumes a molecule of the catalyst **A**, and the rate of decomposition correlates with the efficiency of the chain initiation. Our analysis requires that the decomposition of the catalyst **A** is triggered by productive photochemical initiation only and not by other secondary reactions (which have been never detected during these studies).

The experiments were carried out in identical Schlenk tubes, as they allow a thorough degassing process. The photon flux was calculated utilizing potassium ferrioxalate as actinometer. Two identical Schlenk tubes, containing the actinometer solution and the degassed model reaction (alkylation of **1a** with **2a** catalyzed by **A**), were placed 10 cm away from the light source. They were irradiated together with a 300 W Xenon Lamp operating at 50% of light intensity with a bandpass filter of 450 ± 5 nm. The moles of Fe (II) generated per second ($dx/dt = 1.49 \cdot 10^{-9}$ moles$\cdot s^{-1}$) were measured, and a photon flux ($q^0_{n,p}$) of $3.75 \cdot 10^{-9}$ einstein s^{-1} was determined using Equation S4.

The measurements for the reaction under study were done as follows:
The moles of remaining catalyst **A** were determined by GC measurement (FID detector) using 1,3,5-trimethoxybenzene as internal standard (see Section F1 for details). The moles of catalyst degraded per unit of time were related to the number of photons absorbed and the photons absorbed correlated to the number of incident photons by the use of Equation S4. According to Equation S4, if the moles of catalyst **A** decomposed (x) are plotted versus the moles of incident photons ($q^0_{n,p} \cdot dt$), the slope is equal to: $\mathbf{\Phi \cdot (1-10^{-A(450\ nm)})}$, where Φ is the quantum yield to be determined and *A*(450 nm) is the absorption of the reaction under study. As previously described, *A*(450 nm) was measured using a Shimadzu 2401PC UV-Vis spectrophotometer in 1 mm path quartz in the presence of the bandpass filter of 450 nm employed to carry out the measurements. An absorbance of 1.05 was determined for the reaction with **2a**.

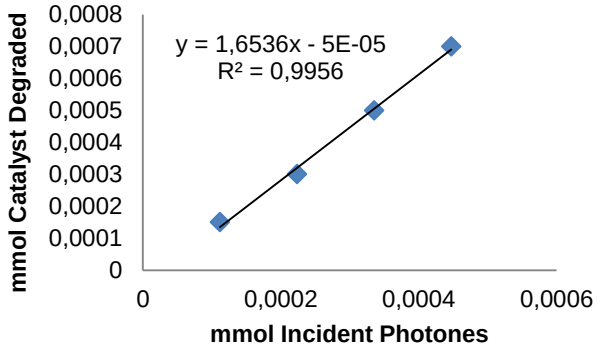

The quantum yield of initiation ($\Phi_{initiation}$) for the photochemical alkylation of butanal **1a** with 2,4-dinitrobenzylbromide **2a** catalyzed by **A** was calculated to be **0.77**, meaning that the actual chain length of the model reaction ($\Phi_{estimated} = \Phi_{measured} / \Phi_{initiation}$) is considerably longer, with a lower limit of **32**.

The same procedure was repeated for the photochemical alkylation of **1a** with bromoacetophenone **2b**, affording a quantum yield of initiation ($\Phi_{initiation}$) of **0.68** (λ = 450 nm). As a result, the actual chain length ($\Phi_{estimated} = \Phi_{measured} / \Phi_{initiation}$) can be approximated to **29**.

G3. Quantum Yield Measurement for the Alkylation with Bromomalonate

The quantum yield measurement was performed following the procedure described in the previous section. Instead of using cuvettes, two identical Schlenk tubes were employed to run the experiments under complete absence of oxygen. The reaction mixtures, containing the actinometer and the model reaction, were placed alongside 10 cm away from a 300 W Xenon lamp operating at 100% of light intensity with a bandpass filter of 400 ± 5 nm. The reaction mixtures were not stirred. The model reaction was prepared as follows: a stock solution was prepared adding 75 mg of the aminocatalyst **A** (0.125 mmol) and 146 µL of 2,6-lutidine (1.25 mmol) to a 5 mL volumetric flask while filling to the mark with acetonitrile (HPLC grade). To 1 mL of this solution, butyraldehyde **1a** (70 µL, 0.75 mmol, 3 equiv.) and ethyl bromomalonate **2c** (43 µL, 0.25 mmol, 1 equiv.) were added. Concomitantly, one 1 mL of this reaction mixture was degassed and used to run the experiment.

Measurements of the actinometer: At 400 nm, the quantum yield (Φ) for Fe^{2+} is 1.13 (*11*). The absorbance of the actinometer solution at 400 nm was measured using a Shimadzu 2401PC UV-Vis spectrophotometer in 1 mm path quartz cuvettes in the presence of the bandpass filter of 400 nm employed to carry out the measurements. An absorbance of 0.288 was obtained. The photon flux $q^0_{n,p}$ was determined to be $3{,}75 \cdot 10^{-9}$ einstein s^{-1}.

Measurements for the alkylation with **2c**: The moles of products formed were determined by ^{1}H NMR spectroscopy. The moles of product per unit of time are related to the number of photons absorbed. The photons absorbed are correlated to the number of incident photons by the use of the Equation S4. According to Equation S4, if we plot the moles of product (x) versus the moles of incident photons ($q^0_{n,p} \cdot dt$), the slope is equal to: $\mathbf{\Phi \cdot (1-10^{-A(400\ nm)})}$ were Φ is the quantum yield and *A*(400 nm) is the absorption of the reaction mixture under study. The absorption was measured using a Shimadzu 2401PC UV-Vis spectrophotometer in 1 mm path quartz in the presence of the bandpass filter of 400 nm employed to carry out the measurements. An absorbance of 0.69 was determined.

The quantum yield (Φ) determined for the photochemical reaction of **1a** with **2c** was **20**.

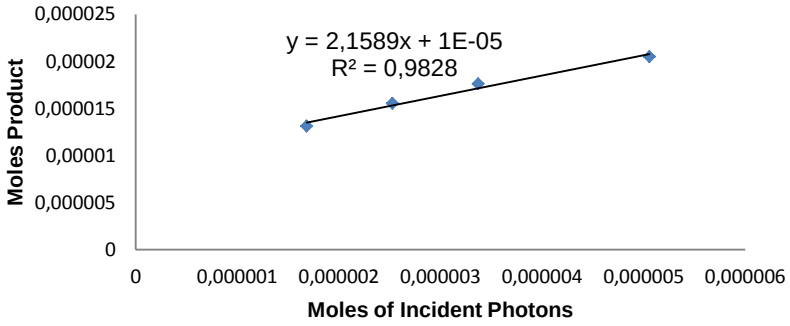

G4. Quantum Yield of the Initiation Step for the Alkylation with Bromomalonate

The quantum yield of the initiation step was measured to better estimate the effective chain length for the reaction of **1a** and diethyl bromomalonate **2c**. The same procedure described in Section G2 was repeated to monitore the decomposition of catalyst **A**.
The photon flux $q^0_{n,p}$ was determined to be $3{,}83 \cdot 10^{-9}$ einstein s^{-1}.

The measurements for the reaction under study were done as follows:
The moles of remaining catalyst **A** were determined by GC measurement (FID detector) using 1,3,5-trimethoxybenzene as internal standard (see Section F1 for details). The moles of catalyst degraded per unit of time are related to the number of photons absorbed. The photons absorbed are correlated to the number of incident photons by the use of the Equation S4. According to Equation S4, if the moles of catalyst **A** decomposed (x) are plotted versus the moles of incident photons ($q^0_{n,p} \cdot dt$), the slope is equal to: $\mathbf{\Phi \cdot (1\text{-}10^{-A(400\ nm)})}$ were Φ is the quantum yield and *A*(400 nm) is the absorption of the reaction mixture under study. The absorption was measured using a Shimadzu 2401PC UV-Vis spectrophotometer in 1 mm path quartz in the presence of the bandpass filter of 400 nm employed to carry out the measurements. An absorbance of 0.69 was determined.

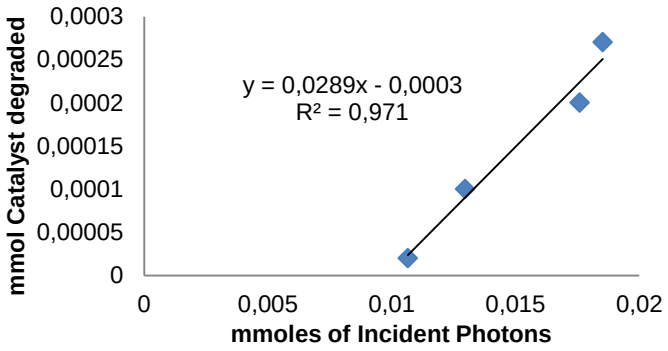

The quantum yield of initiation ($\Phi_{initiation}$) for the photochemical alkylation of butanal **1a** with diethyl bromomalonate **2c** catalyzed by **A** was calculated to be **0.11**. As a result, the actual chain length ($\Phi_{estimated} = \Phi_{measured} / \Phi_{initiation}$) can be approximated to **182**.

H. Investigating the Equilibrium of Enamine Formation

H1. Calculation of the Equilibrium Constant ($K_{enamine}$)

The equilibrium constant for the formation of the enamine, generated upon condensation of the aminocatalyst **A** and butyraldehyde **1a**, was determine by ^{1}H NMR spectroscopy. For this measurements, three solutions containing 0.02 mmol of the catalyst **A** and of 0.02 mmol of 1,3,5-trimethoxybenzene (used as internal standard) and different amounts of **1a** (0.1 mmol, 0.25 mmol and 0.7 mmol) dissolved in 500 µL of dry CD_3CN (previously stored over 4 Å molecular sieves) were prepared. After mixing the components, all the solutions were kept in the dark for 30 minutes to secure equilibration. The relative amount of enamine **I** in solution with respect to the free catalyst **A** was determined by the average of the integration of the following diagnostic peaks: a doublet of doublets at 4.55 ppm (*J* = 9.3, 2.0 Hz, 1H) and a doublet of triplets at 4.09 ppm (*J* = 13.6, 6.8 Hz, 1H) for the enamine **I**; integration of a triplet at 4.40 ppm (*J* = 7.2 Hz, 1H) for catalyst **A** (Figure S23). The amount of water present in solution was calculated by integration of the singlet at 2.13 ppm. The water in solution arises from the condensation process, which generates the enamine, plus the amount of adventitious water originally present in CD_3CN. This is why, as detailed below, the same stock solution of catalyst **A** in dry CD_3CN was used for all the experiments. The total amount of catalyst **A** in solution was compared to the internal standard to ensure that there was no degradation.

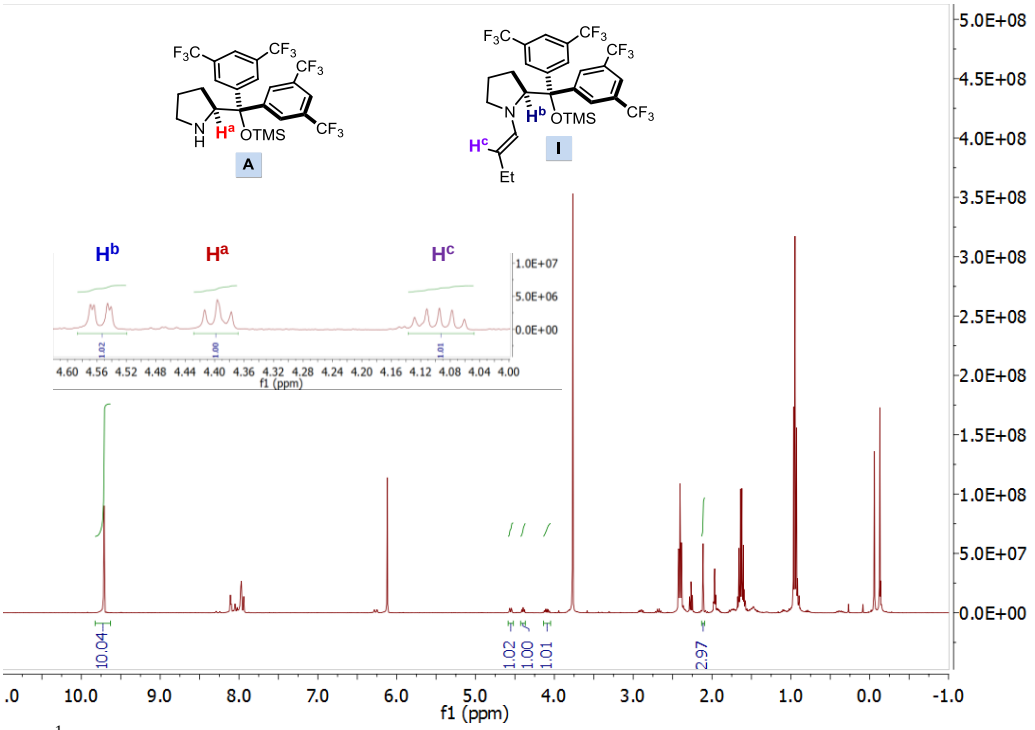

Figure S23. ^{1}H NMR spectra showing the 1.01:1 ratio of enamine **I**:free catalyst **A** for a solution containing: 0.02 mmol of **A** (0.04 M), 0.1 mmol of **1a** (0.2 M) in 0.5 mL of CD_3CN (dried over 4 Å molecular sieves). The ^{1}H NMR spectral window between 4.60 and 4.00 ppm has been enlarged to show diagnostic signals for the enamine **I** and the catalyst **A**.

For these measurements, a stock solution containing 60 mg (0.1 mmol) of **A** and 16.8 mg (0.1 mmol) of 1,3,5-trimethoxybenzene as internal standard in 2.5 mL of CD_3CN (previously dried over 4 Å molecular sieves) was prepared. To 500 μL of this solution (0.04 M in **A**), 10.5 μL of **1a** (0.1 mmol, 0.2 M solution in **1a**) were added. The NMR analysis inferred an enamine **I**/free catalyst **A** ratio of **1.01:1** and a concentration of H_2O of 0.03 M (see Figure S23).

Another solution was prepared from 500 μL of the stock solution 0.04 M in **A** and adding 30 μL of **1a** (0.26 mmol). A **2.32:1** ratio of **I**:**A** was observed and a concentration of H_2O of 0.036 M.

An additional solution was prepared from 500 μL of the stock solution 0.04 M in **A** and adding 80 μL (0.72 mmol of **1a**) of **1a**. A ratio of **I**:**A** of **5.47:1** was observed and a concentration of H_2O of 0.04 M.

With these data and using Equation S5, an equilibrium constants of $\boldsymbol{K_{enamine}}$ **= 0.155 ± 0.002** was determined.

$$K_{enamine} = \frac{[enamine]\cdot[H_2O]}{[free\ catalyst]\cdot[free\ aldehyde]} \qquad \text{(Eq. S5)}$$

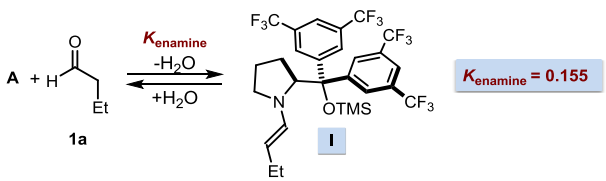

A second, independent set of experiments afforded an equilibrium constant of $\boldsymbol{K_{enamine}}$ **= 0.16 ± 0.02**.

H2. Effect of the EDA Complex Formation on the Enamine Equilibrium

A series of ^{1}H NMR spectroscopic experiments were carried out to study the effect of the EDA complex formation on the enamine formation and its concentration in solution.
Scheme S2 details the system under study:

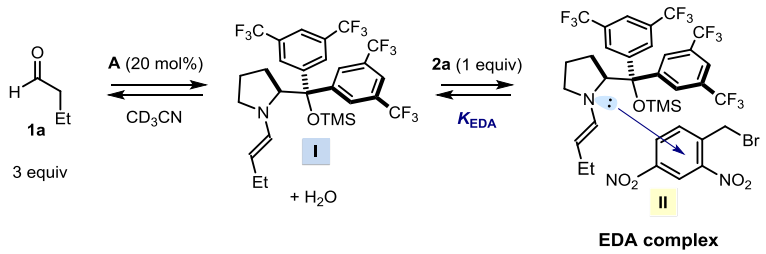

Scheme S2.

The ^{1}H NMR analysis was made on a solution containing 11.9 mg of the aminocatalyst **A** (0.02 mmol), 27 μL of butanal (**1a**) (0.3 mmol) and 12 μL of 2,6-lutidine (0.1 mmol) in 0.5 mL of CD_3CN. Under these conditions (solvent not carefully dried over 4 Å molecular sieves), both enamine **I** and free catalyst **A** were detected in a ratio of 1.2:1 (red spectrum in Figure S24). The free catalyst:enamine ratios were measured by comparing the integrals of the free catalyst peak (triplet at 4.40 ppm, J = 7.2 Hz, 1H) and the diagnostic peaks of the enamine **I** (doublet of doublets at 4.55 ppm (J = 9.3, 2.0 Hz, 1H) and doublet of triplets at 4.09 ppm (J = 13.6, 6.8 Hz, 1H).
Successively, another solution containing 11.9 mg of the aminocatalyst **A** (0.02 mmol), 27 μL of butanal **1a** (0.3 mmol), 12 μL of 2,6-lutidine (0.1 mmol) and 26 mg of **2a** (0.1 mmol) in 0.5 mL of CD_3CN was prepared. This solution was degassed by three cycles of freeze-pump-thaw and its ^{1}H NMR spectrum was recorded (green spectrum in Figure S24). The addition of **2a** induced a shift in the position of the equilibrium toward the enamine **I**, as demonstrated by the 1.8:1 ratio of **I** and free catalyst **A**.
We then used a xenon lamp coupled with a monochromator which, by bringing the light in close contact with the NMR tube through an optical fiber, allowed for the *in situ* illumination of the same sample. When the EDA complex mixture was irradiated *in situ* in the NMR spectrometer (λ = 470±5 nm, irradiance = 28.8 mW/cm^2), a large shift in the position of the enamine equilibrium was immediately observed (3.8:1 ratio of **I**:**A** after 30 seconds of irradiation, blue line in Figure S24). After 60 seconds of irradiation, the signals of the free catalyst **A** could no longer be detected, meaning that the system dramatically shifted towards the enamine **Ib** (purple spectrum in Figure S24).

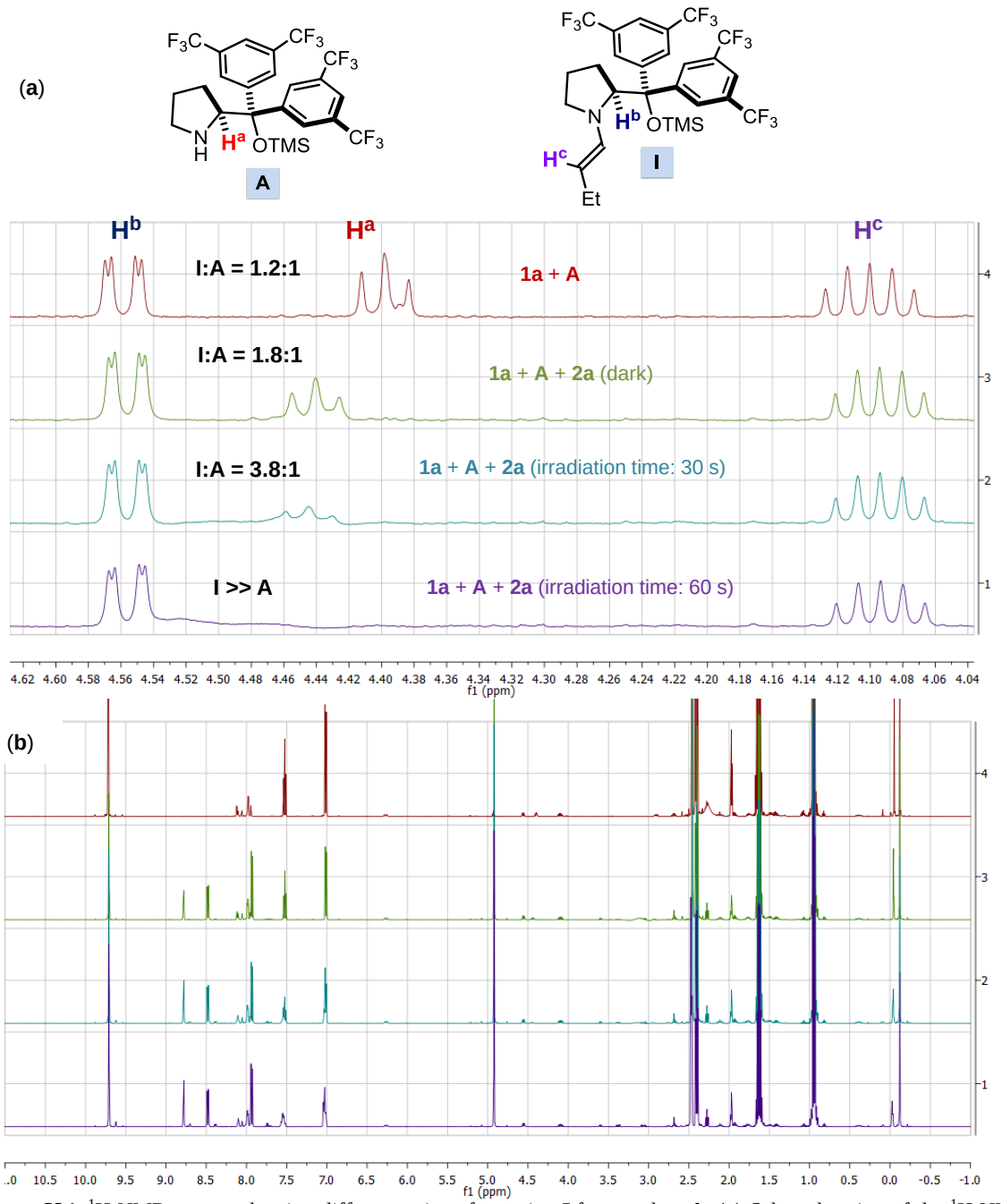

Figure S24. ^{1}H NMR spectra showing different ratios of enamine **I**:free catalyst **A**. (**a**) Selected region of the ^{1}H NMR spectral window between 4.62 and 4.04 ppm showing diagnostic signals for the enamine **I** and the free catalyst **A**. Red spectrum: 0.02 mmol of **A**, 0.3 mmol of **1a**, 0.1 mmol of 2,6-lutidine and 0.5 mL of CD_3CN; green spectrum: 0.02 mmol of **A**, 0.3 mmol of **1a**, 0.1 mmol of 2,6-lutidine, 0.1 mmol of **2a** and 0.5 mL of CD_3CN without illumination; blue spectrum: same mixture as green spectrum while *in situ* irradiating for 30 seconds; purple spectrum: same mixture as green spectrum after 60 seconds of irradiation (λ = 470±5 nm, irradiance = 28.8 mW/cm^2). (**b**) Full ^{1}H NMR spectra. ^{1}H NMR spectroscopic analysis did not allow us to discriminate between the free enamine **I** and the enamine which engages in EDA complex formation with **2a**.

The same experiments were performed replacing **2a** with 2,4-dinitrotoluene **5** (Scheme S3).

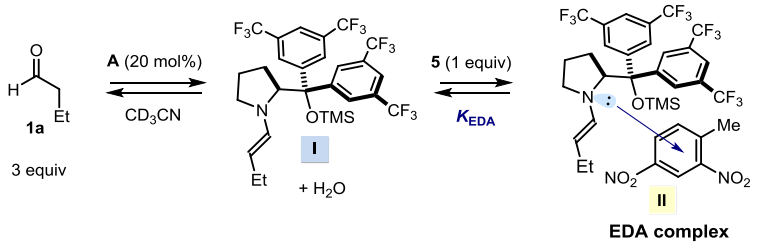

Scheme S3.

5 can act as an acceptor partner in EDA complex formation with the enamine **I**, but it cannot undergo an irreversible fragmentation, since it lacks a suitable leaving group (e.g. the bromine within **2a**). In the dark, the addition of 1 equiv of **5** to a solution of catalyst **A** and butanal **1a** induced a displacement in the equilibrium of the enamine formation, changing the **I**:**A** ratio from 1.2:1 to 1.6:1 (red and green spectra in Figure S25). This is because an EDA complex **II** can be generated, which perturbs the equilibrium of enamine formation. Illumination (λ = 470±5 nm, irradiance = 28.8 mW/cm^2) did not change the concentration of the enamine **I** to any extent (blue spectrum in Figure S25).

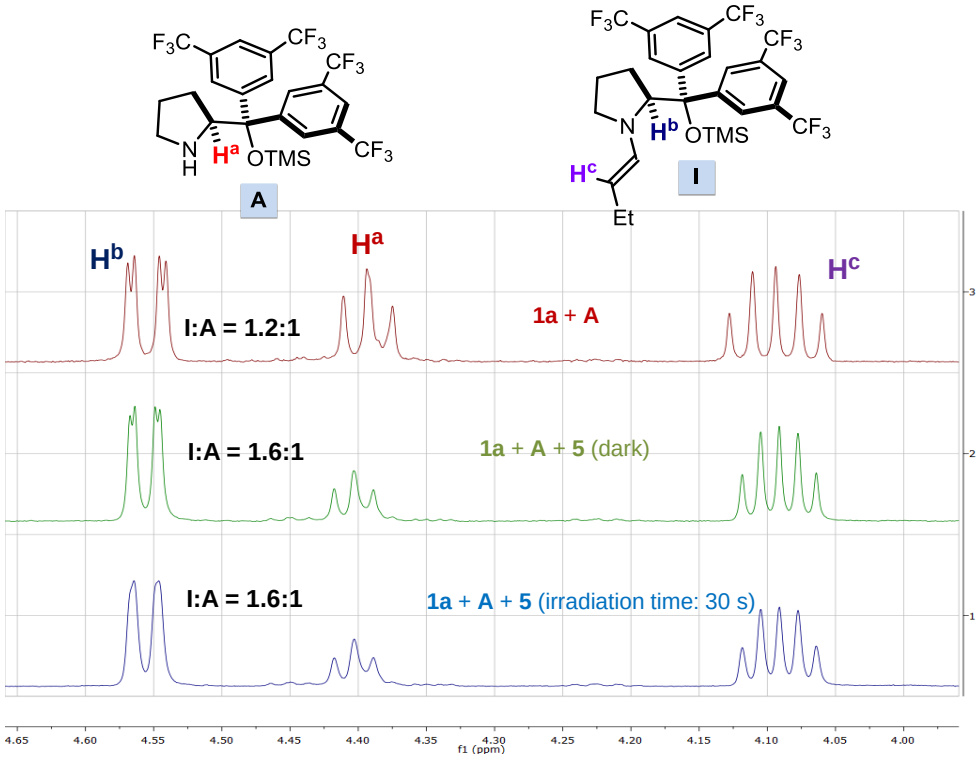

Figure S25. ^{1}H NMR spectra showing different ratios of enamine **I**:free catalyst **A** ratio. Selected region of the ^{1}H NMR spectral window between 4.62 and 4.04 ppm showing diagnostic signals for the enamine **I** and the free catalyst **A**. Red spectrum: 0.02 mmol of **A**, 0.3 mmol of **1a** in 0.5 mL of CD_3CN; green spectrum: 0.02 mmol of **A**, 0.3 mmol of **1a**, 0.1 mmol of 2,4-dinitrotoluene **5** in 0.5 mL of CD_3CN without illumination; blue spectrum: same mixture as green spectrum while *in situ* irradiating for 30 seconds (λ = 470±5 nm, irradiance = 28.8 mW/cm^2).

I. Kinetic Studies

I1. Kinetic Studies for the EDA Complex-mediated Alkylation of Butanal with 2a

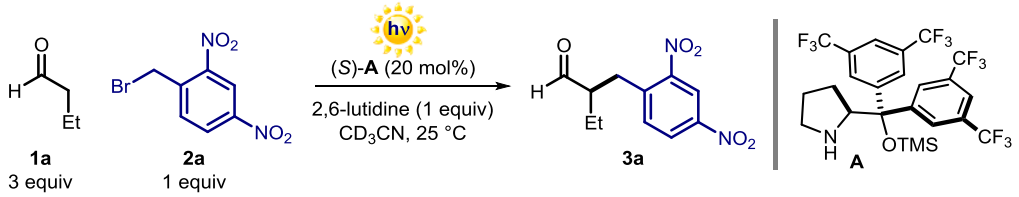

Scheme S4: The EDA complex-mediate alkylation of butanal **1a** with 2,4-dinitrobenzyl bromide **2a**.

Two different procedures, detailed below as Methods A and B, have been used for the initial-rate kinetic measurements.

Method A - *Independent experiments*

Three sets of reactions with identical concentrations of each reactant, except for the reagent whose order is being measured, were carried out in three identical Schlenk tubes. The Schlenk tubes containing the reaction mixtures were positioned laterally, 10 cm away from the light source. They were irradiated with 300 W Xenon Lamp operating at 100% of light intensity (irradiance: 4.7 mW/cm^2) with a bandpass filter at 450 ± 5 nm without stirring. This procedure was repeated 4 times quenching the reactions at different time intervals (this set-up required an independent reaction to be performed for every data-point at different times).

The model reaction was set up utilizing a stock solution containing 360 mg of the aminocatalyst **A** (0.6 mmol) and 15 mg of 1,3,5-trimethoxybenzene (employed as internal standard to measure the conversion of the enamine in solution) dissolved in 6 mL of CD_3CN. To 400 μL of this solution (0.1 M in **A**), 54 μL of butyraldehyde **1a** (0.6 mmol, 3 equiv.), 24 μL of 2,6-lutidine (0.2 mmol, 1 equiv.) and 52 mg of 2,4-dinitrobenzyl bromide **2a** (0.2 mmol, 1 equiv.) were sequentially added. The reaction mixture was thoroughly degassed via freeze pump thaw (x 3 cycles), and the vessel refilled with argon. After irradiating for the indicated time, the conversion of 2,4-dinitrobenzyl bromide **2a** into the final product **3a** was determined by ^{1}H NMR analysis.

These conditions account for the following concentrations: [**A**] = 0.1 M, [**1a**] = 1.5 M and [**2a**] = 0.5 M and [2,6-lutidine] = 0.5 M.

To measure the order with respect to each reactant, we varied the concentration of the reagent under study in the following ranges:

- [**A**] from 0.05 M to 0.2 M.
- [**1a**] from 0.75 M to 3 M.
- [**2a**] from 0.25 M to 1 M.

Method B - *In situ monitoring of the reaction progress*

The reactions were carried out utilizing the same stoichiometry as described in Method A. However, no degassing process was carried out and the reaction vessel was a regular NMR tube. The reactions were irradiated at 470 nm with a 150 W high-stability light xenon lamp Tilluxe P45 coupled to a monochromator for exact wavelength definition (irradiance: 28.8 mW/cm^2 at 2 mm). The monochromator was connected to an optical fiber which was directly introduced into the NMR tube inside the instrument (Bruker, 500 MHz). The conversion of 2,4-dinitrobenzyl bromide **2a** into the final product **3a** was determined by ^{1}H NMR spectroscopy. This process was repeated changing the stoichiometry of the reactants as explained above.

The model reaction was set up utilizing a stock solution containing 72 mg of the aminocatalyst **A** (0.12 mmol) and 3 mg of 1,3,5-trimethoxybenzene (employed as internal standard to measure the conversion of the enamine in solution) dissolved in 6 mL of deuterated acetonitrile. To 500 μL of

this solution (0.02 M in **A**), butyraldehyde **1a** (13.5 µL, 0.15 mmol, 3 equiv.), 2,6-lutidine (6 µL, 0.05 mmol, 1 equiv.) and 2,4-dinitrobenzyl bromide **2a** (13 mg, 0.05 mmol, 1 equiv.) were sequentially added. These conditions account for the following concentrations: [**A**] = 0.02 M, [**1a**] = 0.3 M, [**2a**] = 0.1 M and [2,6-lutidine] = 0.1 M.

To measure the order with respect to each reactant, we used the conditions described above while varying the concentration of the reagent under study in the following ranges:

- [**A**] from 0.01 M to 0.04 M.
- [**1a**] from 0.15 M to 0.6 M.
- [**2a**] from 0.05 M to 0.2 M.

Generally, a faster reaction rate was observed when using method B, a likely consequence of the greater light exposure of the reaction system.

Order dependence in catalyst **A**

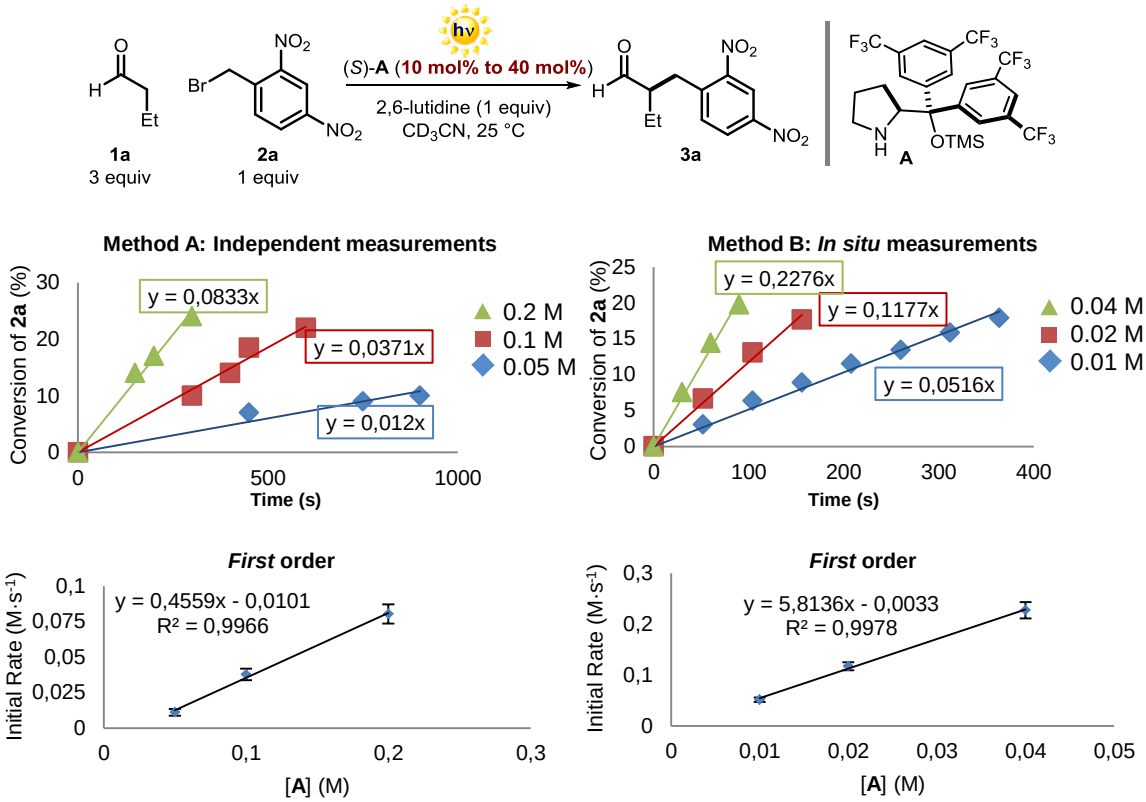

Figure S26. Reaction profiles at different initial concentrations of **A** showing a first-order dependence in [**A**]. Rate constants calculated from the slope of the plots. Reaction profiles using independent measurements (Method A, *left* panel, λ = 450 nm, irradiance = 4.7 mW/cm^2): [**1a**] = 1.5 M; [**2a**] = 0.5 M; [2,6-lutidine] = 0.5 M and [**A**]$_0$ = 0.05 M (blue line), [**A**]$_0$ = 0.1 M (red line) and [**A**]$_0$ = 0.2 M (green line). Reaction profiles using *in situ* measurements (Method B, *right* panel, λ = 470 nm, irradiance = 28.8 mW/cm^2): [**1a**] = 0.3 M; [**2a**] = 0.1 M; [2,6-lutidine] = 0.1 M and [**A**]$_0$ = 0.01 M (blue line), [**A**]$_0$ = 0.02 M (red line) and [**A**]$_0$ = 0.04 M (green line).

As shown in Figure S26, a first-order dependence in [**A**] was determined.

Order dependence in **1a**

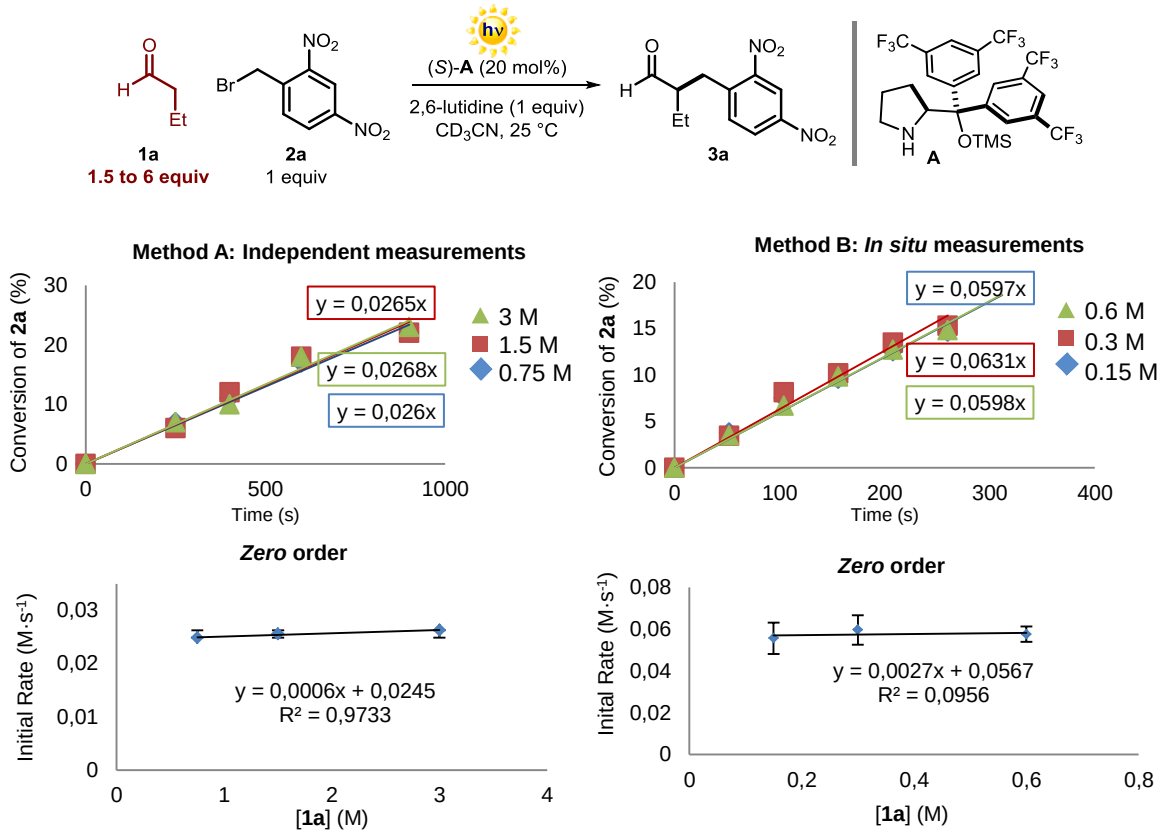

Figure S27. Reaction profiles of initial-rate measurements at different initial concentrations of **1a** showing a zero-order dependence. Rate constants calculated from the slope of the plots. Reaction profiles using independent measurements (Method A, *left* panel, λ = 450 nm, irradiance = 4.7 mW/cm^2): [**A**] = 0.1 M; [**2a**] = 0.5 M; [2,6-lutidine] = 0.5 M and [**1a**]$_0$ = 0.75 M (blue line), [**1a**]$_0$ = 1.5 M (red line) and [**1a**]$_0$ = 3 M (green line). Reaction profiles using *in situ* measurements (Method B, *right* panel, λ = 470 nm, irradiance = 28.8 mW/cm^2): [**A**] = 0.02 M; [**2a**] = 0.1 M; [2,6-lutidine] = 0.1 M and [**1a**]$_0$ = 0.15 M (blue line), [**1a**]$_0$ = 0.3 M (red line) and [**1a**]$_0$ = 0.6 M (green line).

As shown in Figure S27, a zero order dependence in [**1a**] was determined.

Order dependence in **2a**

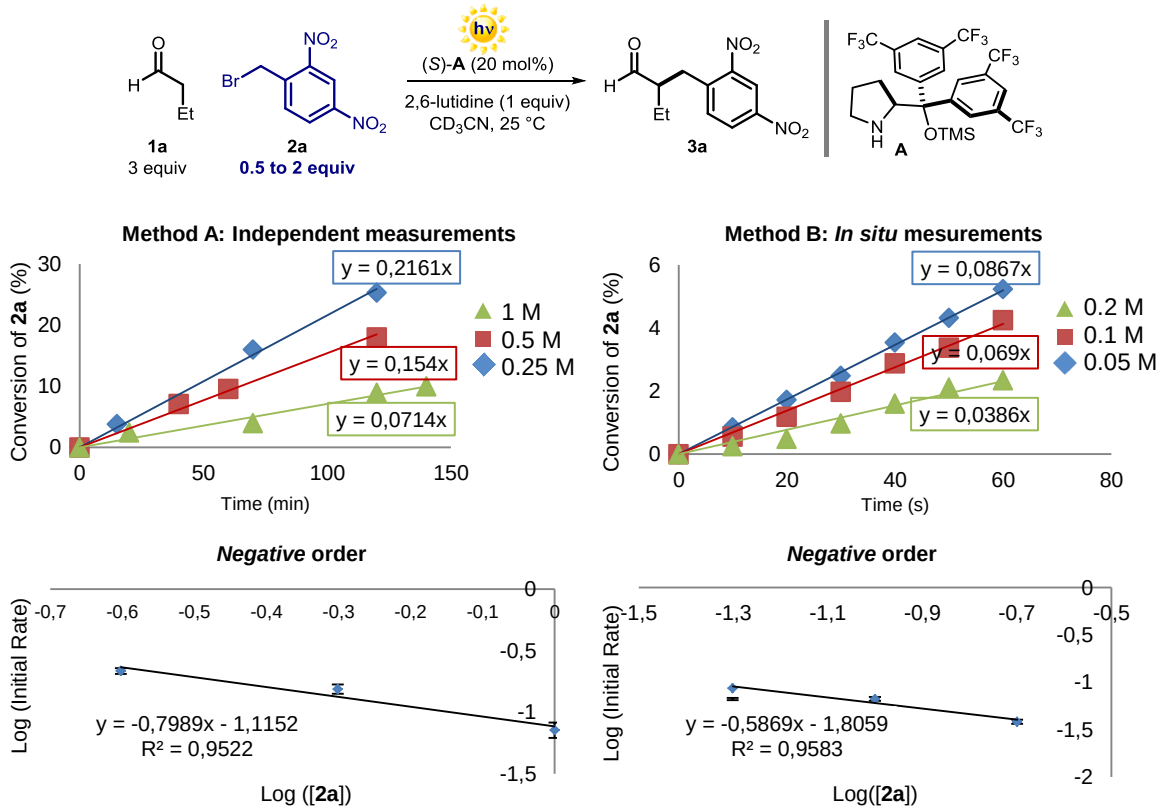

Figure S28. Reaction profiles of initial-rate measurements at different initial concentrations of **2a** showing a negative-order dependence. Rate constants calculated from the slope of the plots. Reaction profiles using independent measurements (Method A, *left* panel, λ = 450 nm, irradiance = 4.7 mW/cm^2): [**A**] = 0.1 M; [**1a**] = 1.5 M; [2,6-lutidine] = 0.5 M and [**2a**]$_0$ = 0.25 M (blue line), [**2a**]$_0$ = 0.5 M (red line) and [**2a**]$_0$ = 1 M (green line). Reaction profiles using *in situ* measurements (Method B, *right* panel, λ = 470 nm, irradiance = 28.8 mW/cm^2): [**A**] = 0.02 M; [**1a**] = 0.3 M; [2,6-lutidine] = 0.1 M and [**2a**]$_0$ = 0.05 M (blue line), [**2a**]$_0$ = 0.1 M (red line) and [**2a**]$_0$ = 0.2 M.

As shown in Figure S28, a negative fractional order dependence in [**2a**] was determined.
The negative dependence was also observed when performing the same *in situ* NMR monitoring of the reaction progress as in Figure S28, right panel, but using a different intensity of irradiation (λ = 470 nm, but irradiance = 3.0 vs 28.8 mW/cm^2), see Figure S29.

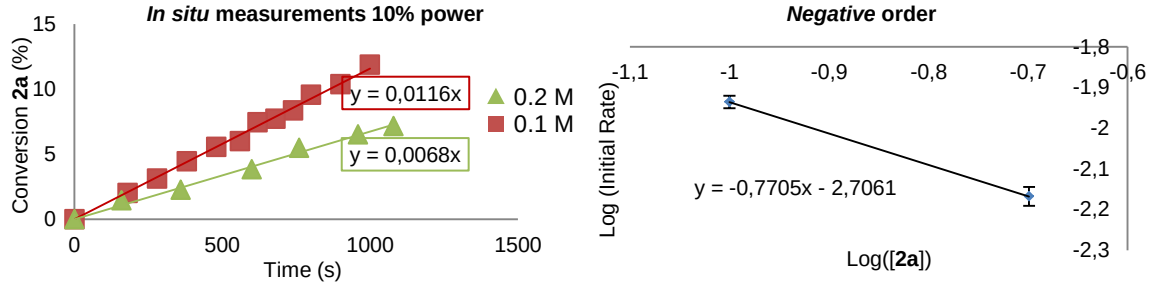

Figure S29. Reaction profiles of initial-rate measurements at different initial concentrations of **2a** showing a fractional negative-order dependence. Rate constants calculated from the slope of the plots. Reaction profiles using *in situ* measurements (λ = 470 nm, irradiance = 3.0 mW/cm^2): [**A**] = 0.02 M; [**1a**] = 0.3 M; [2,6-lutidine] = 0.1 M; [**2a**]$_0$ = 0.1 M (red line) and [**2a**]$_0$ = 0.2 M (green line).

Figure 30 shows that the kinetic data obtained with the different methods overlay when [**A**] is plotted against [**2a**]^{1}·t. The overlay found for plots of [**A**] versus [**2a**]^{1}·*t* establishes a first-order dependence on [**2a**] for the catalyst's disappearance. For more details on the evolution of the catalyst concentration in solution using *in situ* NMR monitoring, see Section F3.

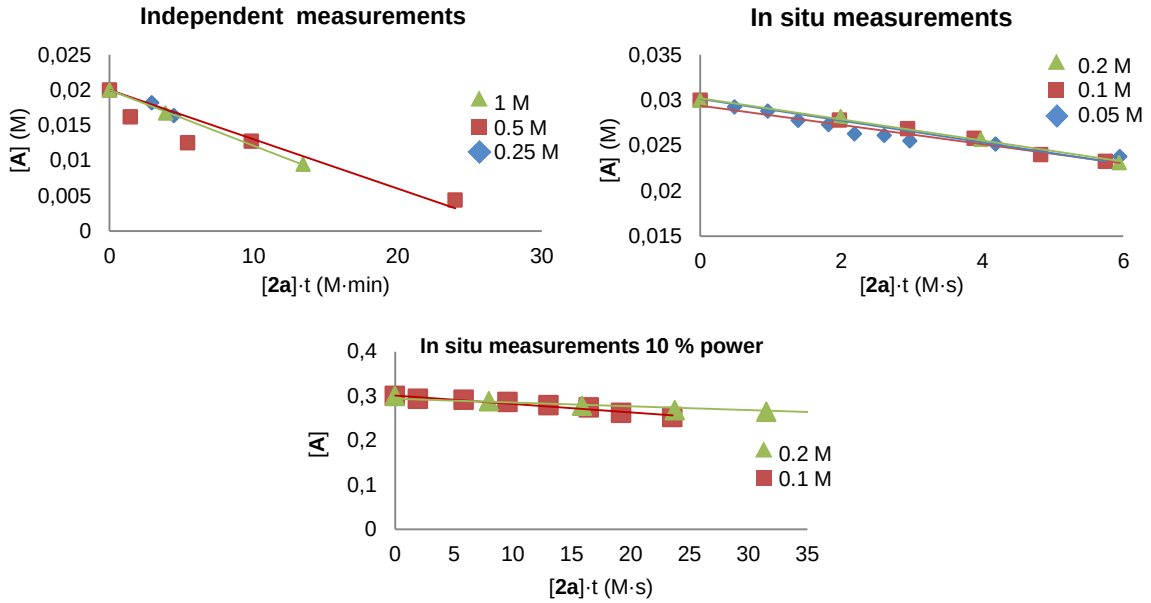

Figure S30. Overlay of plots according to equation 2 in the manuscript for n=1 for reactions containing different initial concentrations of **2a**: [**2a**]$_0$ = 0.25 M (blue line), [**2a**]$_0$ = 0.5 M (red line) and [**2a**]$_0$ = 1 M (green line) (*up left*) and [**2a**]$_0$ = 0.05 M (blue line), [**2a**]$_0$ = 0.1 M (red line) and [**2a**]$_0$ = 0.2 M (green line) (*up right*). [**2a**]$_0$ = 0.1 M (red line) and [**2a**]$_0$ = 0.2 M (green line) (*down*) for reactions irradiated with 10 % power.

Order dependence in H_2O

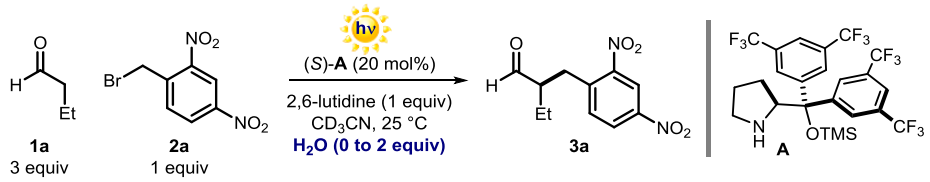

The effect of water on the reaction rate was measured with both the independent measurement approach and *in situ* ^{1}H NMR spectroscopy by adding zero (blue line in Figure S31), one (red line in Figure S31), or two (green line in Figure S31) equivalents of water. The reactions were performed using dried CD_3CN (stored over 4 Å molecular sieves)

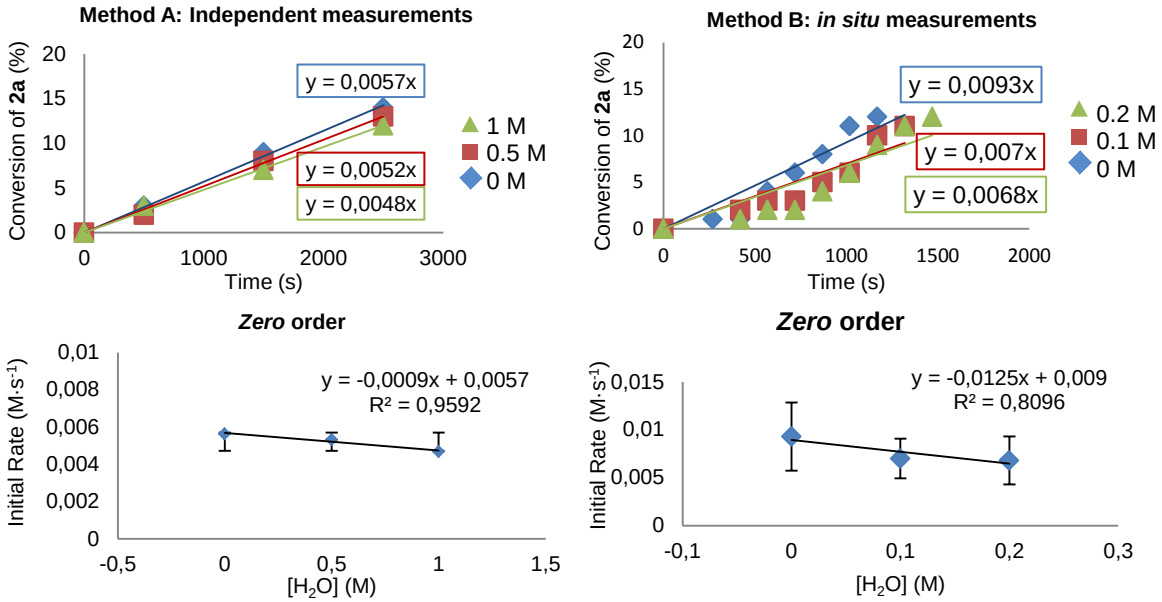

Figure S31. Reaction profiles at different initial concentrations of H_2O. Rate constants calculated from the slope of the plots. Reaction profiles using independent measurements (Method A, *left* panel, λ = 450 nm, irradiance = 4.7 mW/cm^2): [**A**] = 0.1 M; [**1a**] = 1.5 M; [2,6-lutidine] = 0.5 M; [**2a**]$_0$ = 0.5 M and [H_2O]$_0$ ≈ 0 M (blue line), [**H_2O**]$_0$ = 0.5 M (red line) and [**H_2O**]$_0$ = 1.0 M (green line). Reaction profiles using *in situ* measurements (Method B, *right* panel, λ = 470 nm, irradiance = 28.8 mW/cm^2): [**A**] = 0.02 M; [**1a**] = 0.3 M; [2,6-lutidine] = 0.1 M; [**2b**]$_0$ = 0.1 M and [**H_2O**]$_0$ ≈ 0 M (blue line), [**H_2O**]$_0$ = 0.1 M (red line) and [**H_2O**]$_0$ = 0.2 M (green line). Rates determined while varying [**H_2O**]$_0$ using independent measurements at two different irradiation intensities (*down left*) and using *in situ* measurements (*down right*).

As shown in Figure S31, a zeroth-order dependence in [H_2O] was determined.

I2. Kinetic Studies for the EDA Complex-mediated Alkylation of Butanal with 2b

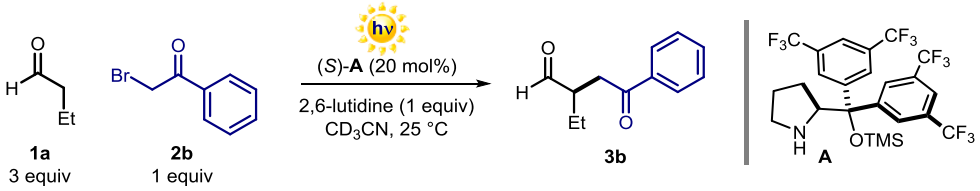

Scheme S5: the EDA complex-mediate alkylation of butanal **1a** with phenacly bromide **2b**.

In order to measure the initial rates of the reaction with **2b**, a series of experiments were carried out in a regular NMR tubes without degassing. The reactions were irradiated at 450 nm with a 150 W high-stability light xenon lamp Tilluxe P45 coupled to a monochromator for exact wavelength definition (irradiance: 23.5 mW/cm^2). This polychromator is connected to an optical fiber which was directly introduced into the NMR tube. This allowed us to monitor the conversion of phenacyl bromide **2b** into the final product **3b** in real time as we can irradiate *in situ* inside an NMR spectrometer (Bruker, 500 MHz). This process was repeated changing the stoichiometry of the reactants.

The model reaction was set up utilizing a stock solution containing 144 mg of the aminocatalyst **A** (0.24 mmol) and 6 mg of 1,3,5-trimethoxybenzene (employed as internal standard to measure the conversion of the enamine in solution) dissolved in 6 mL of CD_3CN. To 500 µL of this solution (0.04 M in **A**), butyraldehyde **1a** (27 µL, 0.3 mmol, 3 equiv.), 2,6-lutidine (12 µL, 0.1 mmol, 1 equiv.) and phenacyl bromide **2b** (20 mg, 0.1 mmol, 1 equiv.) were sequentially added. These conditions account for the following concentrations: [**A**] = 0.04 M, [**1a**] = 0.6 M and [**2b**] = 0.2 M and [2,6-lutidine] = 0.2 M.

To measure the order with respect to each reactant, we varied the concentration of the reagent under study in the following ranges:

- [**A**] from 0.02 M to 0.08 M.
- [**1a**] from 0.3 M to 1.2 M.
- [**2b**] from 0.1 M to 0.4 M.

Order dependence in catalyst **A**

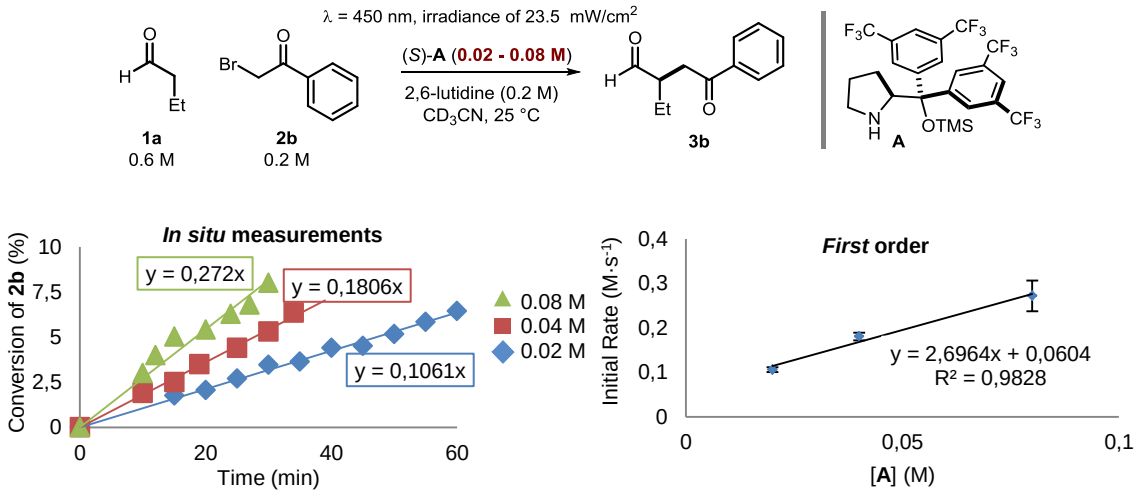

Figure S32. Reaction profiles of initial-rate measurements at different initial concentrations of **A** showing a first-order dependence: $[\mathbf{A}]_0$ = 0.02 M (blue line), $[\mathbf{A}]_0$ = 0.04 M (red line) and $[\mathbf{A}]_0$ = 0.08 M (green line) (*left*). Rates determined while varying $[\mathbf{A}]_0$ (*right*).

As shown in Figure S32, a first-order dependence in [**A**] was determined.

Order dependence in **1a**

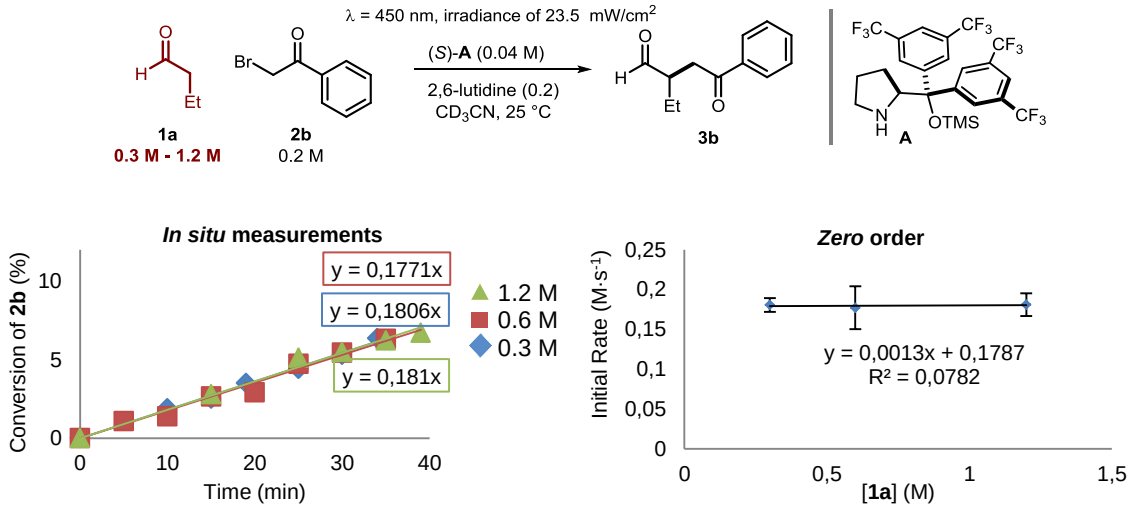

Figure S33. Reaction profiles at different initial concentrations of **1a**: $[\mathbf{1a}]_0$ = 0.3 M (blue line), $[\mathbf{1a}]_0$ = 0.6 M (red line) and $[\mathbf{1a}]_0$ = 1.2 M (green line) (*left*). Rates determined while varying $[\mathbf{1a}]_0$ (*right*).

As shown in Figure S33, a zero-order dependence in [**1a**] was determined.

Order dependence in **2b**

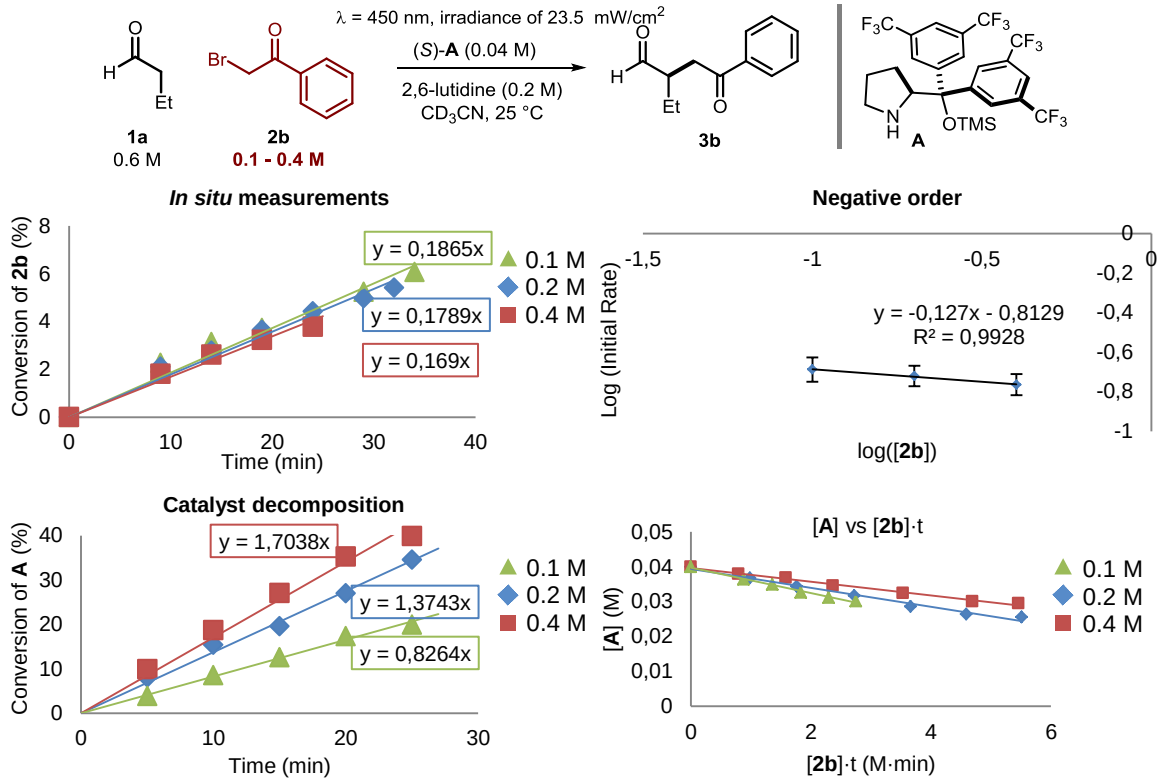

Figure S34. Experiments performed at different initial concentrations of **2b**: $[\mathbf{2b}]_0$ = 0.4 M (red line), $[\mathbf{2b}]_0$ = 0.2 M (blue line) and $[\mathbf{2b}]_0$ = 0.1 M (green line). Reaction profiles used for initial rate calculations (*up left*). Logarithmic plot of the rates determined while varying $[\mathbf{2b}]_0$ (*up right*). Evolution of the catalyst **A** concentration for the same reactions (*down left*), measured from the concentration of enamine **I** in solution. Overlay of plots according to Equation 2 in the main manuscript for n=1 for reactions containing different initial concentrations of **2b.**

As shown in Figure S34, a negative order in **2b** was determined. Furthermore, catalyst degradation was observed over time. The overlay found for plots of [**A**] versus $[\mathbf{2b}]^1 \cdot t$ (n = 1 in Equation 2 of the main manuscript) establishes a first-order dependence on [**2b**] for the catalyst's disappearance (Figure S34, right bottom panel).

We then wanted to measure the real effect of [**2b**] on the rate of alkylation leading to product **3b**, discounting the effects of catalyst **A** degradation in the initiation regime. The plotting of the kinetic data (Figure S35) according to Equation 4 of the main manuscript shows a good fit for $[\mathbf{3b}] \cdot [\mathbf{A}]^{-1}$ vs $[\mathbf{2b}]^{0.5} \cdot t$ (n = 0.5 in Equation 4). This indicates a *positive* half-order dependence on [**2b**].

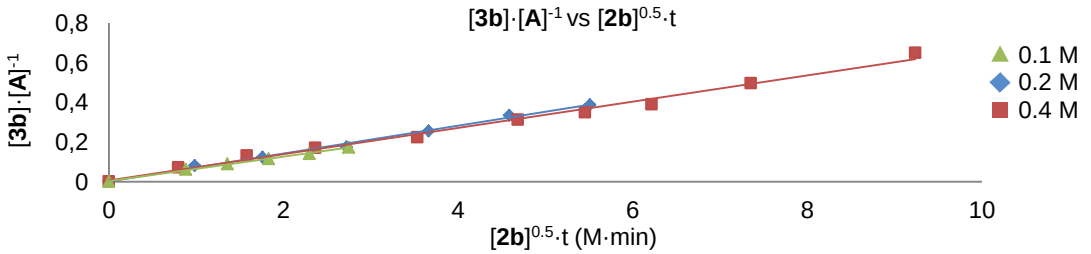

Figure S35. Overlay of plots, according to Equation 4 in the main manuscript, for n=0.5 ($[\mathbf{3b}] \cdot [\mathbf{A}]^{-1}$ vs $[\mathbf{2b}]^n \cdot t$) for reactions containing different initial concentrations of **2b**: $[\mathbf{2b}]_0$ = 0.4 M (red line), 0.2 M (blue line) and $[\mathbf{2b}]_0$ = 0.1 M (green line).

I3. Kinetic Studies for the Alkylation of Butanal with Bromomalonate 2c

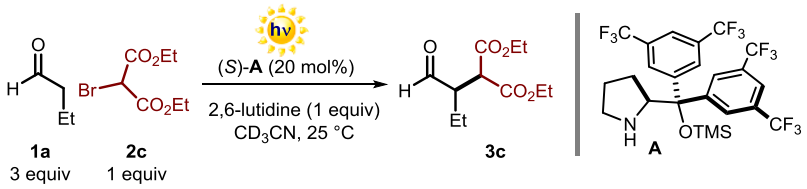

Scheme S6: alkylation of butanal **1a** with bromomalonate **2c**.

Two different procedures, detailed below as Methods A and B, have been used for the initial-rate kinetic measurements.

Method A - *Independent experiments*

Sets of three reactions with identical concentrations of every reactant except for the specie whose order is being measured were carried out in three identical Schlenk tubes. The Schlenk tubes containing the reaction mixtures were positioned alongside, 10 cm away from the light source. They were irradiated with a 300 W Xenon lamp operating at 100% of light intensity (irradiance: 300 mW/cm^2; 150 mW/cm^2 when 50% power was applied) with a cut-off filter at 385 nm ($\lambda \geq 385$ nm) without stirring. This procedure was repeated 4 times quenching the reactions at different time intervals (this set-up required an independent reaction to be performed for every data-point at different times).

The reaction was set up utilizing a stock solution containing 360 mg of the aminocatalyst **A** (0.6 mmol) and 15 mg of 1,3,5-trimethoxybenzene (employed as internal standard to measure the conversion of the enamine in solution), dissolved in 6 mL of CD_3CN. To 100 μL of this solution (0.1 M in **A**), butyraldehyde **1a** (13.5 μL, 0.15 mmol, 3 equiv.), 2,6-lutidine (6 μL, 0.05 mmol, 1 equiv.) and ethyl bromomalonate **2c** (8.5 μL, 0.05 mmol, 1 equiv.) were sequentially added. The reaction mixture was thoroughly degassed via freeze pump thaw (x 3 cycles), and the vessel refilled with argon. After irradiating for the indicated time, the conversion of ethyl bromomalonate **2c** was measured by ^{1}H NMR analysis. These conditions account for the following concentrations: [**A**] = 0.1 M, [**1a**] = 1.5 M, [**2c**] = 0.5 M and [2,6-lutidine] = 0.5 M.

To measure the order with respect to each reactant, we used the conditions described above while varying the concentration of the reagent under study in the following ranges:

- [**A**] from 0.05 M to 0.15 M.
- [**1a**] from 0.75 M to 3 M.
- [**2c**] from 0.25 M to 1 M.

Method B - *In situ monitoring of the reaction progress*

The reactions were carried out using the same stoichiometry as described in Method A. However, no degassing process was carried out and the reaction vessel was a regular NMR tube. The reactions were irradiated at 400 nm with a 150 W high-stability light xenon lamp Tilluxe P45 coupled to a monochromator for exact wavelength definition (irradiance: 20.4 mW/cm^2 at 2 mm). The monochromator was connected to an optical fiber which was directly introduced into the NMR tube inside the instrument (Bruker, 500 MHz). The conversion of bromomalonate **2c** into the final product **3c** was determined by ^{1}H NMR spectroscopy. This process was repeated changing the stoichiometry of the reactants.

The model reaction was set up utilizing a stock solution containing 72 mg of the aminocatalyst **A** (0.12 mmol) and 3 mg of 1,3,5-trimethoxybenzene (employed as internal standard to measure the conversion of the enamine in solution) dissolved in 6 mL of CD_3CN. To 500 μL of this solution

(0.02 M in **A**), butyraldehyde **1a** (13.5 µL, 0.15 mmol, 3 equiv.), 2,6-lutidine (6 µL, 0.05 mmol, 1 equiv.) and ethyl bromomalonate **2c** (8.5 µL, 0.05 mmol, 1 equiv.) were sequentially added. These conditions account for the following concentrations: [**A**] = 0.02 M, [**1a**] = 0.3 M, [**2c**] = 0.1 M and [2,6-lutidine] = 0.1 M.

To measure the order with respect to each reactant, we used the conditions described above while varying the concentration of the reagent under study in the following ranges:

- [**A**] from 0.01 M to 0.04 M.
- [**1a**] from 0.15 M to 0.6 M.
- [**2c**] from 0.05 M to 0.2 M.

Generally, a faster reaction rate was observed when using method B, a likely consequence of the greater light exposure of the reaction system.

Order dependence in catalyst **A**

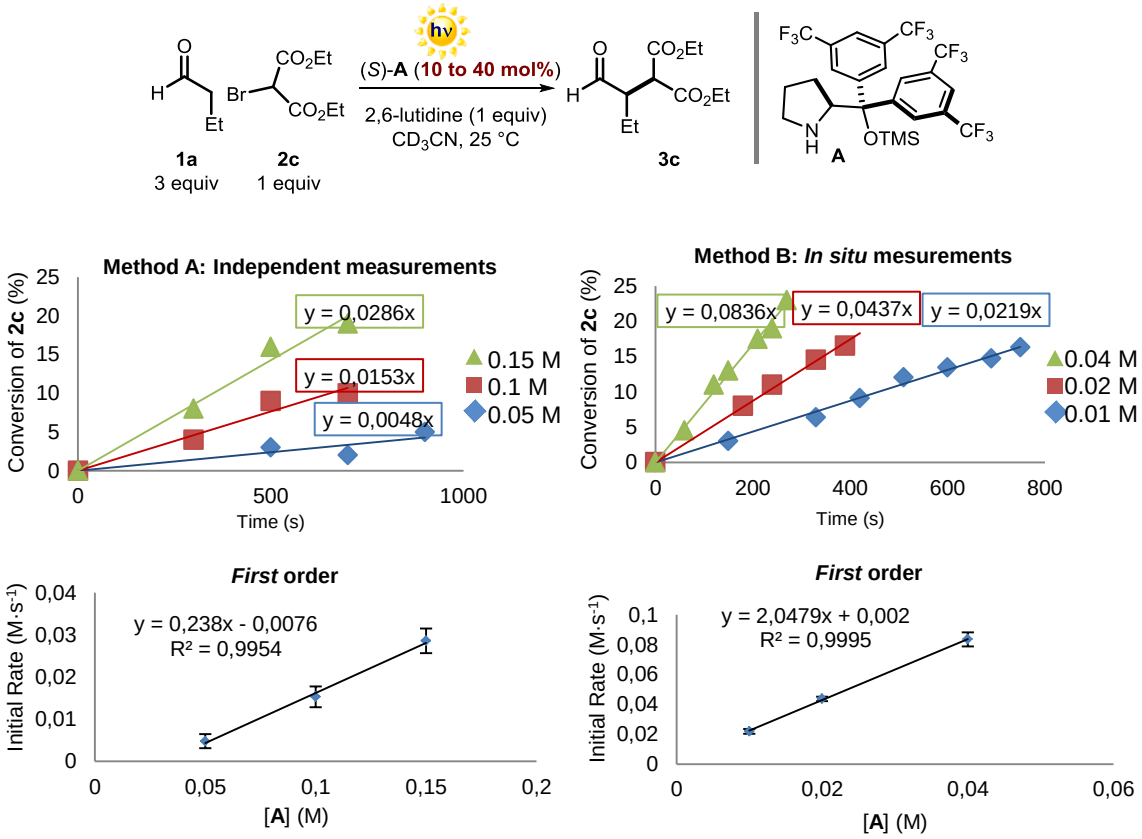

Figure S36. Reaction profiles at different initial concentrations of **A** showing a first-order dependence in [**A**]. Rate constants calculated from the slope of the plots. Reaction profiles using independent measurements (Method A, *left* panel, $\lambda \geq 385$ nm (*cut-off*), irradiance = 300 mW/cm^2): [**1a**] = 1.5 M; [**2c**] = 0.5 M; [2,6-lutidine] = 0.5 M and $[\mathbf{A}]_0$ = 0.05 M (blue line), $[\mathbf{A}]_0$ = 0.1 M (red line) and $[\mathbf{A}]_0$ = 0.15 M (green line). Reaction profiles using *in situ* measurements (Method B, *right* panel, λ = 400 nm, irradiance = 20.4 mW/cm^2): [**1a**] = 0.3 M; [**2c**] = 0.1 M; [2,6-lutidine] = 0.1 M and $[\mathbf{A}]_0$ = 0.01 M (blue line), $[\mathbf{A}]_0$ = 0.02 M (red line) and $[\mathbf{A}]_0$ = 0.04 M (green line).

As shown in Figure S36, a first-order dependence in [**A**] was determined.

Order dependence in **1a**

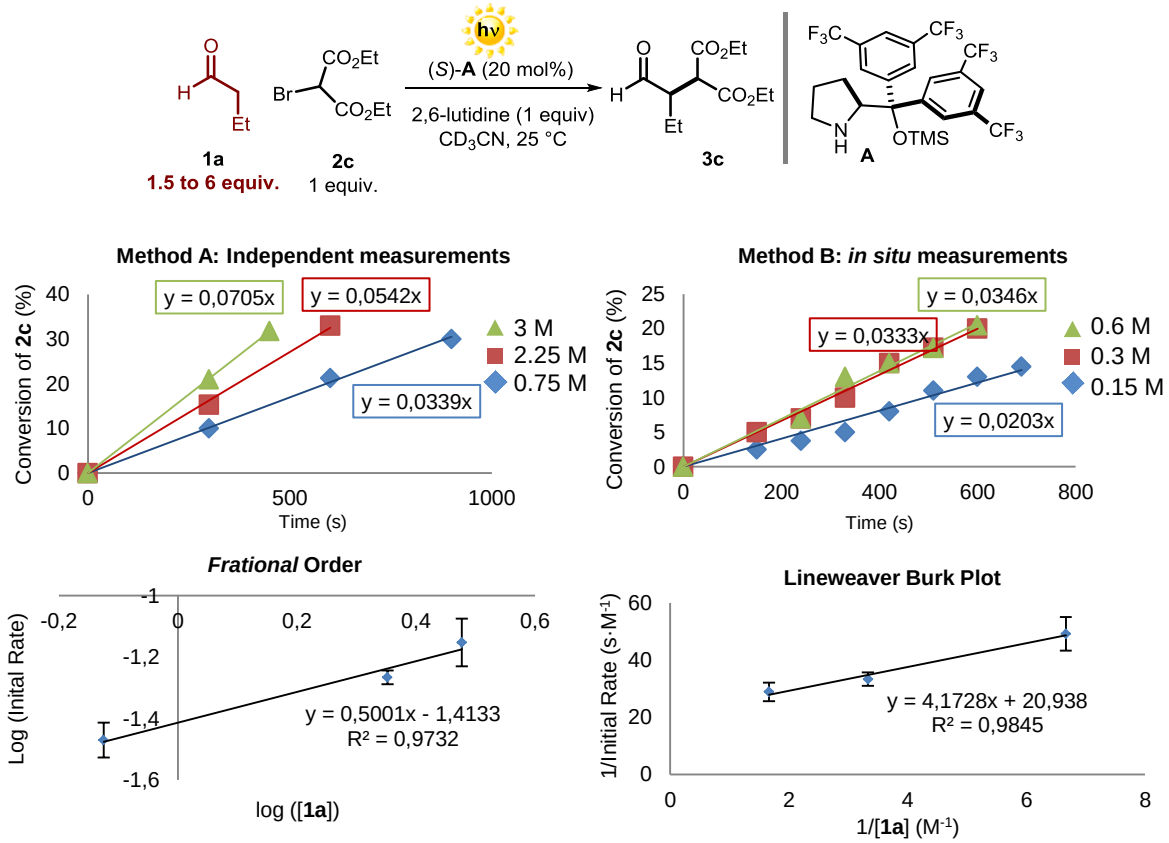

Figure S37. Reaction profiles at different initial concentrations of **1a**. Rate constants calculated from the slope of the plots. Reaction profiles using independent measurements (Method A, *left* panel, $\lambda \geq 385$ nm (*cut-off*), irradiance = 300 mW/cm^2): [**A**] = 0.1 M; [**2c**] = 0.5 M; [2,6-lutidine] = 0.5 M and [**1a**]$_0$ = 0.75 M (blue line), [**1a**]$_0$ = 2.25 M (red line) and [**1a**]$_0$ = 3.0 M (green line). Reaction profiles using *in situ* measurements (Method B, *right* panel, λ = 400 nm, irradiance = 20.4 mW/cm^2): [**A**] = 0.02 M; [**2c**] = 0.1 M; [2,6-lutidine] = 0.1 M and [**1a**]$_0$ = 0.15 M (blue line), [**A**]$_0$ = 0.3 M (red line) and [**A**]$_0$ = 0.6 M (green line). Logarithmic plot of the rates determined while varying [**1a**]$_0$ using independent measurements (*down left*). Lineweaver Burk plot for the rates determined while varying [**1a**]$_0$ using *in situ* measurements (*down right*).

As shown in Figure S37, a half-order dependence in [**1a**] was determined using the method of independent measurements. A saturation kinetic profile was observed instead when using the *in situ* monitoring. This is presumably because of catalyst decomposition pathways triggered by the presence of oxygen in the system, as *in situ* monitoring did not allow for complete de-oxygenation of the reaction medium (see Section F for further details on the catalyst decomposition). When using the independent measurement approach, instead, we *did not observe any catalyst degradation* before than 20% conversion.

Order dependence in **2c**

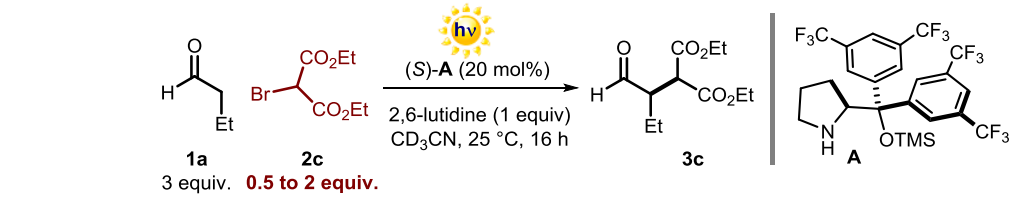

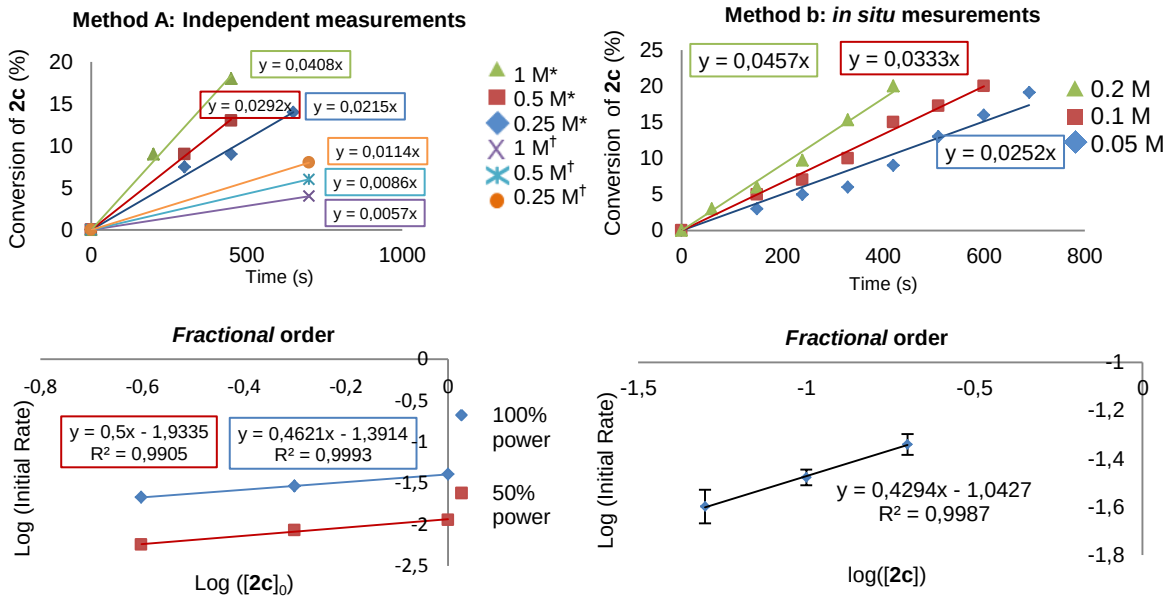

Figure S38. Reaction profiles at different initial concentrations of **2c**. Rate constants calculated from the slope of the plots. Reaction profiles using independent measurements (Method A, *left* panel, λ ≥ 385 nm (*cut-off*)): we performed two sets of experiments under the same conditions, but using a different intensity of irradiation: *reaction irradiated with **100% power**, irradiance = 300 mW/cm^2: [**A**] = 0.1 M; [**1a**] = 1.5 M; [2,6-lutidine] = 0.5 M and [**2c**]$_0$ = 0.25 M (blue line), [**2c**]$_0$ = 0.5 M (red line) and [**2c**]$_0$ = 1.0 M (green line). †Reaction irradiated with **50% power**, irradiance = 150 mW/cm^2: [**A**] = 0.1 M; [**1a**] = 1.5 M; [2,6-lutidine] = 0.5 M and [**2c**]$_0$ = 0.25 M (orange line), [**2c**]$_0$ = 0.5 M (light blue line) and [**2c**]$_0$ = 1.0 M (purple line).
Reaction profiles using *in situ* measurements (Method B, *right* panel, λ = 400 nm, irradiance = 20.4 mW/cm^2): [**A**] = 0.02 M; [**1a**] = 0.3 M; [2,6-lutidine] = 0.1 M and [**2c**]$_0$ = 0.05 M (blue line), [**2c**]$_0$ = 0.1 M (red line) and [**2c**]$_0$ = 0.2 M (green line). Logarithmic plot of the rates determined while varying [**2c**]$_0$ using independent measurements at two different irradiation intensities (*down left*) and using *in situ* measurements (*down right*).

As shown in Figure S38, a half-order dependence with respect to **2c** was observed.

Order dependence in H_2O

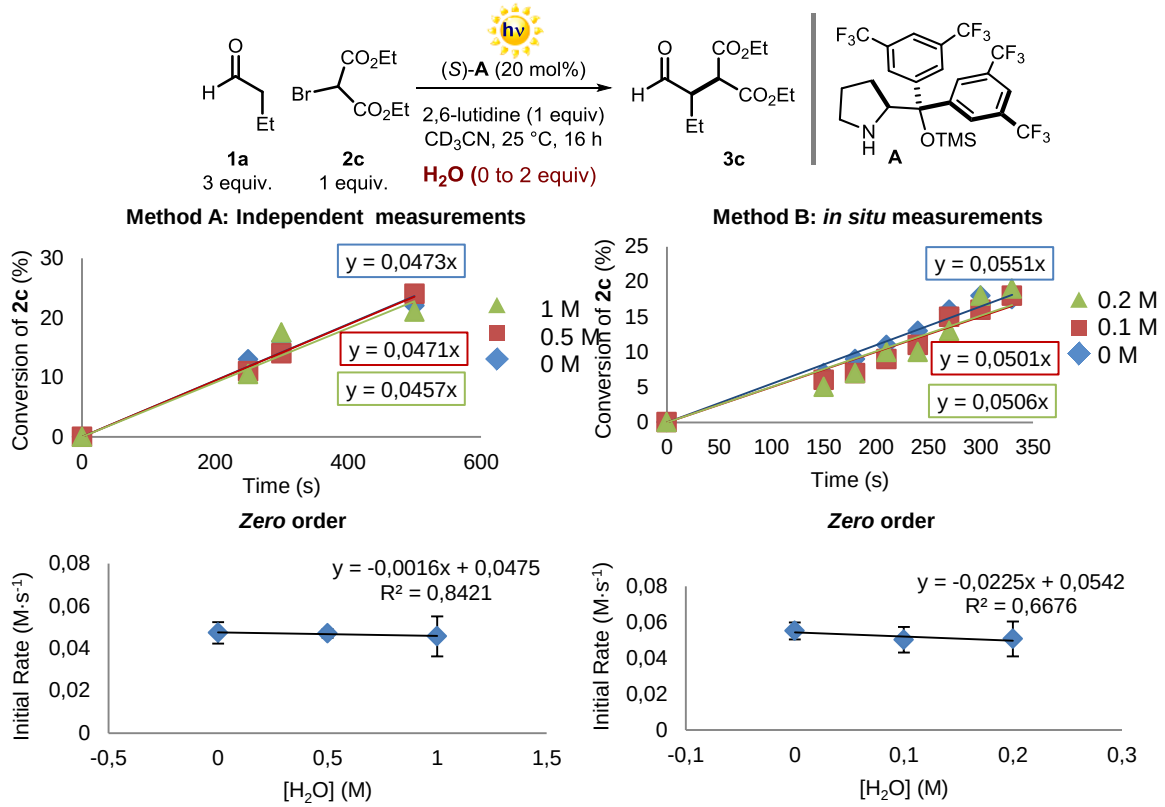

Figure S39. Reaction profiles at different initial concentrations of H_2O. Rate constants calculated from the slope of the plots. Reaction profiles using independent measurements (Method A, *left* panel, $\lambda \geq 385$ nm (*cut-off*), irradiance = 300 mW/cm^2): [**A**] = 0.1 M; [**1a**] = 1.5 M; [2,6-lutidine] = 0.5 M; [**2c**]$_0$ = 0.5 M and $[H_2O]_0 \approx 0$ M (blue line), $[H_2O]_0$ = 0.5 M (red line) and $[H_2O]_0$ = 1.0 M (green line). Reaction profiles using *in situ* measurements (Method B, *right* panel, λ = 400 nm, irradiance = 20.4 mW/cm^2): [**A**] = 0.02 M; [**1a**] = 0.3 M; [2,6-lutidine] = 0.1 M; [**2c**]$_0$ = 0.1 M and $[H_2O]_0 \approx 0$ M (blue line), $[H_2O]_0$ = 0.1 M (red line) and $[H_2O]_0$ = 0.2 M (green line). Rates determined while varying $[H_2O]_0$ using independent measurements at two different irradiation intensities (*down left*) and using *in situ* measurements (*down right*).

As shown in Figure S39, a zeroth-order dependence in $[H_2O]$ was determined.

J. Cyclic Voltammetry

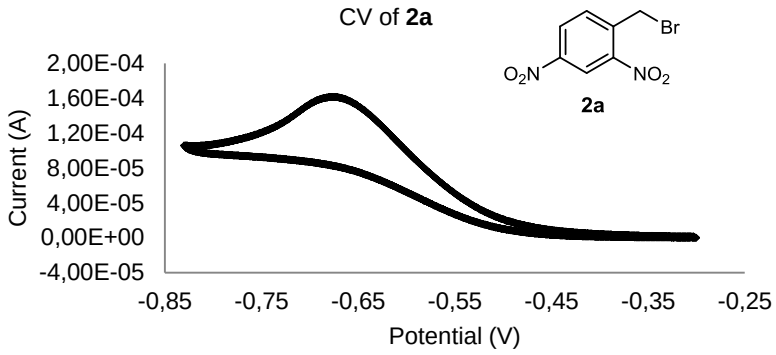

Figure S40. Cyclic voltammogram of 2,4-dinitrobenzyl bromide **2a** [0.02 M] in [0.1 M] $TBAPF_6$ in CH_3CN. Sweep rate: 50 mV/s. Pt electrode working electrode, Ag/AgCl (NaCl saturated) reference electrode, Pt wire auxiliary electrode. E_p^{red} = -0.66 V**.**

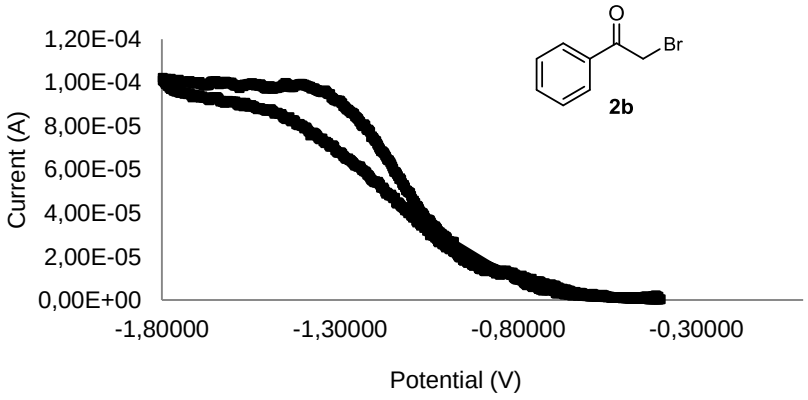

Figure S41. Cyclic voltammogram of phenacyl bromide **2b** [0.02 M] in [0.2 M] $TBAPF_6$ in CH_3CN. Sweep rate: 10 mV/s. Pt electrode working electrode, Ag/AgCl (NaCl saturated) reference electrode, Pt wire auxiliary electrode. Irreversible reduction. E_p^{red} = -1.35 V**.**

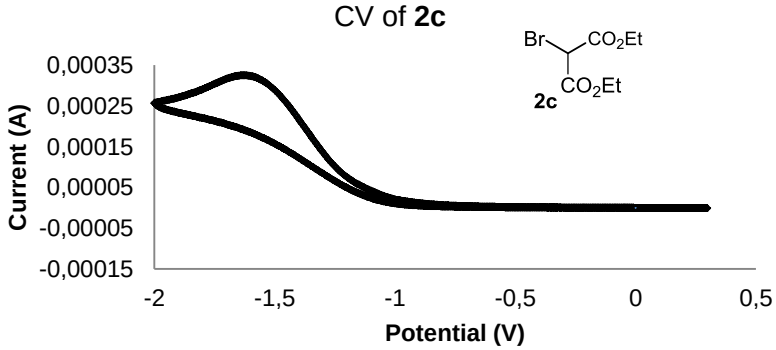

Figure S42. Cyclic voltammogram of diethyl bromomalonate **2c** [0.05 M] in [0.1 M] $TBAPF_6$ in CH_3CN. Sweep rate: 50 mV/s. Pt electrode working electrode, Ag/AgCl (NaCl saturated) reference electrode, Pt wire auxiliary electrode. Irreversible reduction. E_p^{red}= -1.69 V**.**

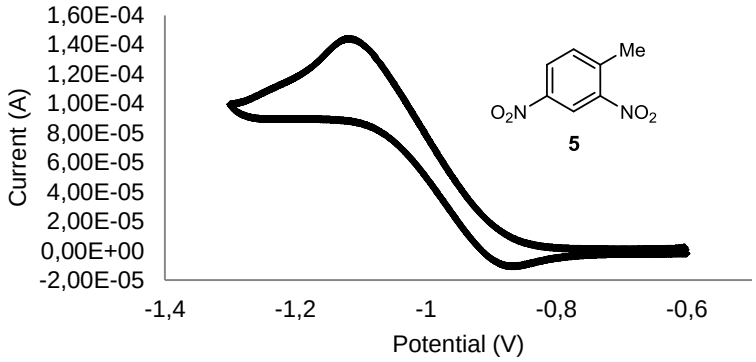

Figure S43. Cyclic voltammogram of 2,4-dinitrotoluene **5** [0.02 M] in [0.1 M] $TBAPF_6$ in CH_3CN. Sweep rate: 20 mV/s. Pt electrode working electrode, Ag/AgCl (NaCl saturated) reference electrode, Pt wire auxiliary electrode. E_p^{red} = -1.10 V, quasi-reversible reduction potential**.**

K. Characterization of the Iminium Ion IX

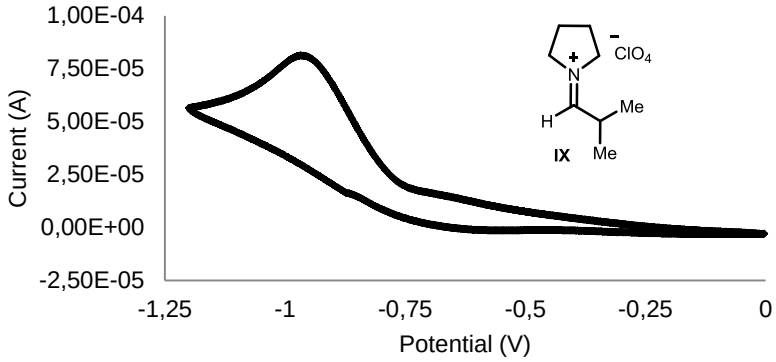

Figure S44. Cyclic voltammogram of the iminium ion **IX** [0.02 M] in [0.1 M] $TBAPF_6$ in CH_3CN. Sweep rate: 10 mV/s. Pt electrode working electrode, Ag/AgCl (NaCl saturated) reference electrode, Pt wire auxiliary electrode. Irreversible reduction. E_p^{red}= -0.95 V**.** The sample measured contained trace amounts of *iso*butyraldehyde and pyrrolidine perchlorate. Cyclic voltammograms of both compounds did not show any reduction till -2.0 V, thus unambiguously assigning the observed pick in Figure S44 to the reduction of **IX**.

Compound **IX** was synthesized from pyrrolidine, perchloric acid and isobutyraldehyde according to (*14*). The pyrrolidine perchlorate salt was prepared by adding 3 mmol of pyrrolidine (0.025 mL) to a solution of 3 mmol of perchloric acid (0.026 mL of a 70% solution) in 1 mL of ether. A slightly yellow precipitate formed, which was filtered and washed with dry ether. The pyrrolidinium perchlorate salt was used for the following step without further purification. Pyrrolidinium perchlorate (0.23 mmol, 40 mg) was suspended in 2 mL of dry ether and freshly distilled *iso*butryladehyde (1 mmol, 0.91 mL) was added. After the addition, the precipitate dissolved while the slow precipitation of a white solid was observed. The reaction was stirred overnight at room temperature. The precipitate was washed with dry hexane (10 mL) under argon and then dried using high vacuum pump. The iminium ion **IX** was obtained in a 23% yield (12 mg) as a white solid.

^{1}H NMR (400 MHz, CD_3CN): δ 8.16 (d, *J* = 9.2 Hz, 1H), 4.07 (t, *J* = 7.0 Hz, 2H), 3.94 (t, *J* = 7.0 Hz, 2H), 2.93 (dh, *J* = 9.2, 6.6 Hz, 1H), 2.13 (m, 4H), 1.24 (d, *J* = 6.6 Hz, 6H).

^{13}C NMR (101 MHz, CD_3CN) δ 180.90, 58.62, 52.25, 32.33, 23.98, 23.63, 17.10.

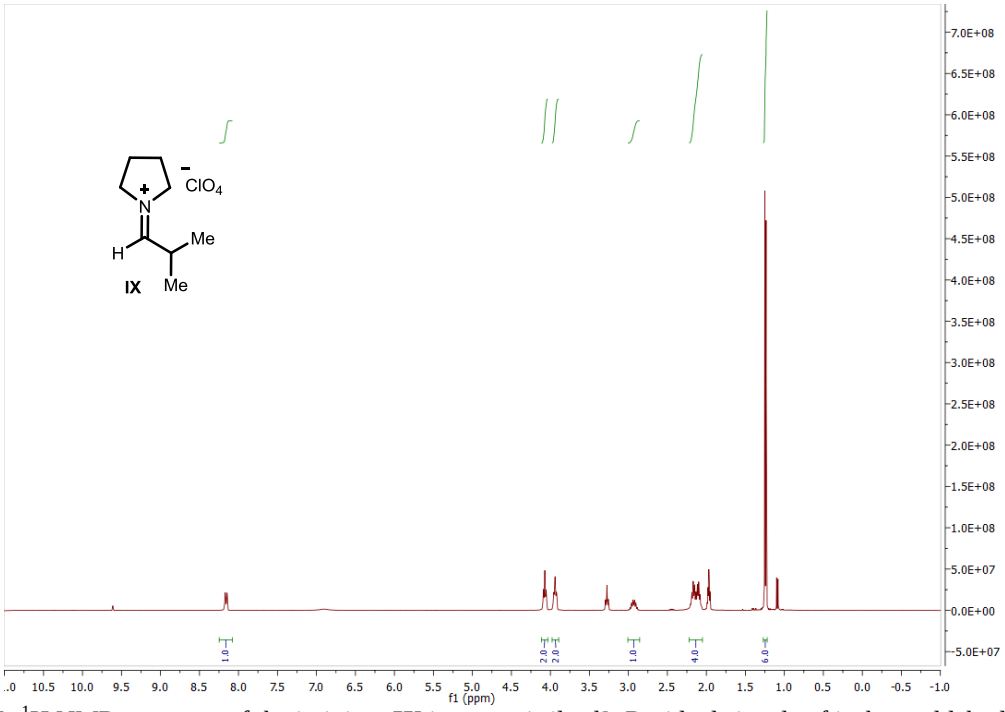

Figure S45: ^{1}H NMR spectrum of the iminium **IX** in acetonitrile-*d3*. Residual signals of isobutyraldehyde, pyrrolidin-1-ium perchlorate and the acetonitrile-*d3* are observed.

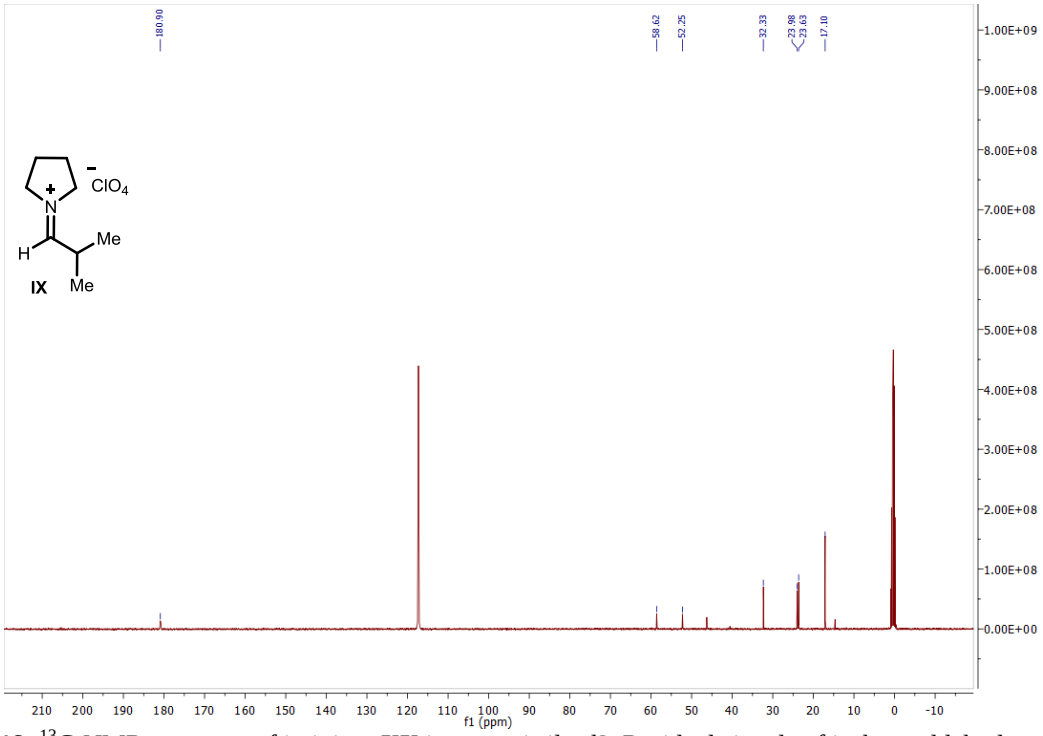

Figure S46: ^{13}C-NMR spectrum of iminium **XX** in acetonitrile-*d3*. Residual signals of isobutyraldehyde, pyrrolidin-1-ium perchlorate and the acetonitrile-*d3* are observed.

L. References

1. Jan, T.; Dupas, B.; Floner, D.; Moinet, C. *Tetrahedron lett.* **2002**, *43*, 5949–5952.
2. Silvi, M.; Arceo, E.; Jurberg, I. D.; Cassani, C.; Melchiorre, P. *J. Am. Chem. Soc* **2015**, *137*, 6120−6123.
3. Arceo, E.; Jurberg, I. D.; Álvarez-Fernández, A.; Melchiorre, P. *Nature Chem.* **2013**, *5*, 750–756.
4. A. Fürstner, M. Bonnekessel, J.T. Blank, K. Radkowski, G. Seidel, F. Lacombe, B. Gabor, A. Mynott, *Chem. Eur. J.* **2007**, *13*, 8762.
5. Rosokha, S. V.; Kochi, J. K. *Acc. Chem. Res.* **2008**, *41*, 641.
6. Job, P. *Ann. Chem.* **1928**, *9*, 113-203.
7. Benesi, H. A.; Hildebrand, J. H. *J. Am. Chem. Soc.* **1949**, *71*, 2703-2707.
8. J. R. Lakowicz *Principles of Fluorescence Spectroscopy,* chap. 3, pp. 52-93, Plenum Press, New York 1983.
9. G. J. Kavarnos *Fundamentals of photoinduced electron transfer* chap. 1, pp 29 VCH Publishers 1993.
10. V. Balzani, P. Ceroni, A. Juris, *Photochemistry and photophysics*, chapter 4, pp. 103, Wiley-VCH, 2014.
11. S. Murov, L., *Handbook of Photochemistry*, Marcel Dekker, New York, **1973**
12. a) Braslavsky, S. E. Glossary of terms used in photochemistry, (IUPAC Recommendations 2006). *Pure and Applied Chemistry* **2007**, *79*, 293-465. b) Sun, L. Bolton, J. R. *J. Phys. Chem.***1996**, *100*, 4127-4134.
13. Hamai, S.; Hirayama, F. *J. Phys. Chem.* **1983**, *87*, 83-89.
14. Leonard, N. J.; Paukstelis, J. V. *J. Org. Chem.* **1963**, *28*, 3021-3024.